CHALMERS
UNIVERSITY OF TECHNOLOGY

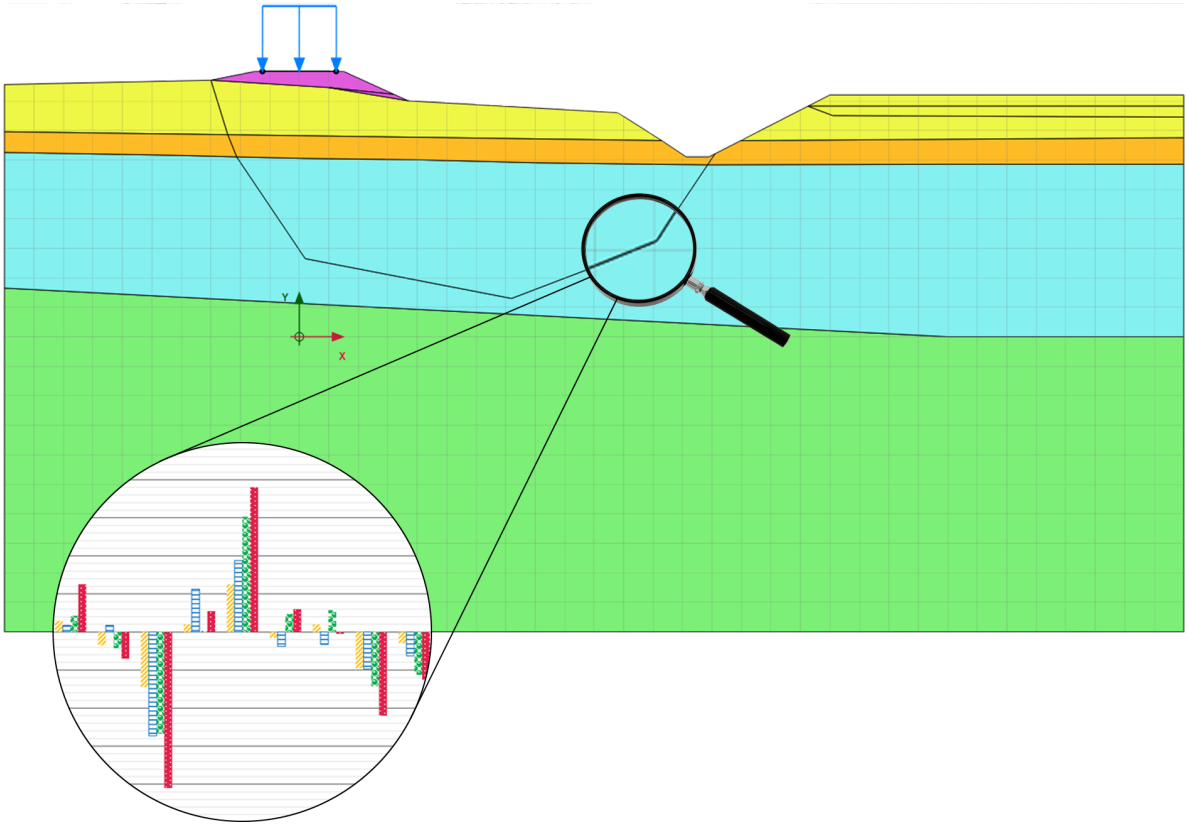

Global Sensitivity Analysis of the Perniö test embankment

Numerical study on the Creep-SCLAY1S model parameters

Master's thesis in the Master's programme Infrastructure and Environmental Engineering

BEHRANG ALIKHANZADEH ALAMDARI
SIMON LARSSON

DEPARTMENT OF ARCHITECTURE AND CIVIL ENGINEERING
CHALMERS UNIVERSITY OF TECHNOLOGY
Gothenburg, Sweden 2021
www.chalmers.se

Master's thesis 2021

Global Sensitivity Analysis of the Perniö test embankment

Numerical study on the Creep-SCLAY1S model parameters

BEHRANG ALIKHANZADEH ALAMDARI
SIMON LARSSON

CHALMERS
UNIVERSITY OF TECHNOLOGY

Department of Architecture and Civil Engineering
Division of Geology and Geotechnics
Chalmers University of Technology
Gothenburg, Sweden 2021

Global Sensitivity Analysis of the Perniö test embankment
Numerical study on the Creep-SCLAY1S model parameters
BEHRANG ALIKHANZADEH ALAMDARI
SIMON LARSSON

Supervisors: Hossein Tahershamsi, Jelke Dijkstra, Department of Architecture and Civil Engineering
Examiner: Jelke Dijkstra, Department of Architecture and Civil Engineering
Industry supervisor: Tara Wood, Ramboll

Master's Thesis 2021
Department of Architecture and Civil Engineering
Division of Geology and Geotechnics
Chalmers University of Technology
SE-412 96 Gothenburg
Telephone +46 31 772 1000

Cover: Visualization of the geometry used for the model, and the results of the fractional factorial design.

Typeset in LaTeX
Printed by Chalmers Reproservice
Gothenburg, Sweden 2021

Global Sensitivity Analysis of the Perniö test embankment
Numerical study on the Creep-SCLAY1S model parameters
BEHRANG ALIKHANZADEH ALAMDARI & SIMON LARSSON
Department of Architecture and Civil Engineering
Chalmers University of Technology

Abstract

Construction of railway embankments on soft soil can be a complex problem. Several numerical models have been proposed to evaluate the behaviour of embankments on soft soils. However, several uncertainties arising from the models used and the underlying experimental data remain. These uncertainties find their origin in the non-linear hydro-mechanical response of (soft) soils, that is affected by the loading history. In this thesis, factorial design is used to quantify the most significant model parameters of Creep-SCLAY1S model which have the most influence on the (predicted) stability of the Perniö Embankment. The study concludes that the parameters connected to destructuration and compressibility of natural clays are important when dealing with slope stability of an embankment on soft soils. Furthermore, the study shows that a maximum of 40 % increase and 44 % decrease would be predicted numerically if the magnitude of the evaluated parameters are altered around 15 % of their centre value. It is also argued that more triaxial tests in extension should be performed for this type of geotechnical problem that leads to a shallow failure plane.

Keywords: Fractional factorial design, Full factorial design, Python, pyDOE2,
Design of Experiments, Perniö, Failure test, Embankment, Creep-SCLAY1S, PLAXIS.

Acknowledgements

This Master's thesis report is written by two students at the Master's programme Infrastructure and Environmental Engineering at Chalmers University of Technology.

We as authors would like to give our most sincere gratitude to Jelke Dijkstra, professor in the Division of Geology and Geotechnics at Chalmers, for his support, guidance and dedicated work as examiner.

We would also like to thank Hossein Tahershamsi, doctoral student in the Division of Geology and Geotechnics at Chalmers, for his encouragement, challenging us and thorough work as supervisor.

Our deepest appreciation goes to Tara Wood, Head of business research and development, and Nathali Cuotto Sánchez, Geotechnical engineer, at Ramboll, for sharing their valuable experience and geotechnical expertise throughout this thesis.

Last but not least, we want to thank our fellow Master's students David Tran and Yohanes Armediaz for critically evaluating this thesis and opposing us during the presentation.

Behrang Alikhanzadeh Alamdari, Gothenburg, June 2021
Simon Larsson, Gothenburg, June 2021

Contents

List of Figures

List of Tables

List of Notations

Abbreviations

IL OT	Incremental Loading Oedometer Test
POP	Pre Overburden Pressure *[kPa]*
OCR	Over-Consolidation Ratio *[-]*
NCS	Normal Consolidation Surface
CSS	Current Stress Surface
FVT	Field Vane Test
CPTU	Cone Penetration Test with pore water pressure reader
FEM	Finite Element Analysis
GSA	Global Sensitivity Analysis
LSA	Local Sensitivity Analysis

Greek letters

κ^*	Modified swelling index	$-$
λ_i^*	Modified intrinsic compression index	$-$
μ_i^*	Intrinsic modified creep index	$-$
τ	Reference time	*Time*
ω	Absolute effectiveness of rotational hardening	$-$
ω_d	Relative deviatoric effectiveness of rotational hardening	$-$
ξ	Absolute rate of destructuration	$-$
ξ_d	Relative rate of destructuration	$-$
χ_0	Initial bonding	$-$
α_0	Initial anisotropy	$-$
ν'	Poisson's ratio	$-$
ν'_{ur}	Poisson's ratio for unloading-reloading	$-$
ϕ	Friction angle	$^\circ$
ϕ'	Effective friction Angle	$^\circ$
ψ	Dilatancy angle	$^\circ$
γ_{sat}	Saturated unit weight	kN/m^3
γ_{unsat}	Unsaturated unit weight	kN/m^3

Roman letters

M_c	Slope of critical state line in compression	–
M_e	Slope of critical state line in extension	–
c	Cohesion	kN/m^2
c'_{ref}	Effective reference cohesion	kN/m^2
E'	Young's modulus	kN/m^2
e_0	Initial void ratio	–
K_0^{nc}	Value of K0 for a normally consolidated state	–
K_x	Horizontal hydraulic conductivity	m/day
K_y	Vertical hydraulic conductivity	m/day
C_k	Change of permeability	–
$K_{0,x}$	Coefficient of lateral earth pressure in x direction	–
$K_{0,z}$	Coefficient of lateral earth pressure in z direction	–

1
Introduction

Train railway networks in Finland are considered as one of the oldest railway constructions in the Nordic countries. The first Finnish railway was built in 1869 and connected Finland to Russia (Vozniak et al., 2018). In later years, the speed and weight of the trains have increased and the demand of having better public transportation systems are high due to population growth. Railways are also an important transportation system since it is one of the safest ways of transportation. For instance, fatality risk of 0.035 (per 100 million passenger-kilometres) for air and rail travel are recorded for the years between 2001 and 2002 (ETSC, 2003). In many areas, the public transportation systems need to be renovated to be able to address the high demands of traffic (Eckhardt and Rantala, 2012). Hence, for the dimensioning of embankments for future needs it is important to facilitate possibly faster, heavier and more frequent trains. Correct dimensioning will also lead to more sustainable infrastructure, both in terms of economic, ecologic and social impact. Construction of railway embankments on soft soil is considered as a challenging issue for geotechnical engineers. Large settlements can occur during and after the construction phase, and stability needs to be ensured throughout the life time. Hence, it is important to have a better understanding of the soil behaviour beneath the embankments and the models used for quantification of this behaviour.

The determination of model parameters is a crucial step in establishing the safety of embankments. Soft clays are known as complex materials that show significant movement when responding to an applied load. The movement of clay is dependent on many factors, such as (degree of) consolidation, destructuration, anisotropy, creep, bonding that lead to non-linear behaviour. The model parameters that describe this soil behaviour need to be understood and considered to ensure safety (Gras et al., 2018).

In the report of Mansikkamäki, 2015, the Perniö embankment failure test was simulated using different constitutive models for the soil. The study concluded that the Creep-SCLAY1S material model showed the most realistic soil behaviour, when comparing to the Soft Soil and Modified Cam Clay models (Mansikkamäki, 2015). Some of the Creep-SCLAY1S model parameters can be determined by laboratory tests, meanwhile others must be calculated using complex formulas and/or curve fitting (Gras et al., 2018).

The available experimental data and other information on the site can be limited, samples can be disturbed before being tested, and other uncertainties entering the

process are not always well understood. It, therefore, can be difficult to evaluate the value of parameters with certainty, especially throughout a larger area in a real-world project. Hence, it is essential to find out how results are affected by input parameters, those include the parameters of the constitutive model and other parameters that define the numerical analysis.

1.1 Aim and objectives

The main objective of this study is to carry out a global sensitivity analysis of the Creep-SCLAY1S model parameters to quantify which parameters affect the stability of an embankment on soft soils. Two methods of factorial design will be utilized for the global sensitivity analysis of a comprehensive Finite Element simulation of the Perniö test embankment, for which both a detailed Site Investigation and a well document failure load test are available.

1.2 Limitations

The limitations connected to this thesis will be discussed in this section.

- A limitation is that the Perniö embankment test site was located where there previously had been an old railway. Hence, the soil has already been under a previous load, creating uncertainties regarding the loading history of the soil.
- A full factorial design should be utilized for the entire study to do a thorough sensitivity analysis. However, for a full factorial design with 13 parameters, a total of $2^{13} = 8192$ simulations would be necessary. To reduce the computational time and to screen out non-important parameters, first a fractional factorial design will be designed before progressing with a full factorial design on the reduced parameter set.
- The Mohr-Coulomb model parameters were assumed and adjusted with typical and reasonable values of Finnish and Scandinavian soils. This is due to lack of data for the coarse-grained materials at the test site.

1.3 Methodology

A literature review regarding previous studies of the test site was conducted first. Then, a detailed site description, the determination of model parameters and soil properties, and the finite element method, FEM, modelling of the failure test were performed. Additionally, detailed background of sampling, in-situ investigations, laboratory tests, and data calibration were conducted. The literature study was performed towards the different constitutive models used. The modelling was carried out using PLAXIS 2D, which is a widely used commercial finite element code used in geotechnical engineering. The version of PLAXIS 2D used was from 2019. Different techniques were discussed for performing the sensitivity analysis, which resulted in performing two-level fractional factorial design and full factorial design.

2

Global Sensitivity Analysis

A sensitivity analysis is defined as the distribution of uncertainties in output model to different uncertainties in the input model (Saltelli, 2004). The term of model can be defined as numerical or otherwise.

The model results are highly dependent on model parameters. The sensitivity analysis is aimed to identify the influence of input parameters on results. It can help to determine and eliminate the insignificant inputs. Also, it can be used to assess the sensitive inputs to have further research on them, thereby reducing uncertainties. Additionally, it is utilized to identify which input parameters are correlated the most towards output variability (Iman and Helton, 1988).

Sensitivity analysis can play an important role while making a critical decision throughout the results of the studies (Christopher Frey and Patil, 2002). Nowadays, sensitivity analyses are performed in different science fields such as medical, social, engineering and economics. Thereby, by determining the uncertainties in models, extra research and data gathering can be expected for future studies (Cullen et al., 1999). There are multiple techniques that have been suggested for performing sensitivity analyses, where the general process are listed as below (Hamby, 1994):

- A model needs to be determined.
- Defining the dependent and independent variables.
- Evaluating the probability of each input parameters.
- For some sensitivity analysis an input matrix needs to be generated based on sampling method.
- Evaluating the correlation of input and output parameters.

Generally, sensitivity analyses can be classified as below:

- Local Sensitivity Analysis, LSA: The method is defined as the evaluation of the local effects of the input variables on the model outputs (Sudret, 2008). Also the interactions between inputs are not considered. It is generally concentrate on the impact of uncertain input parameters around a specific points.
- Global Sensitivity Analysis, GSA: The method is defined as the evaluation of the output uncertainties which are resulted due to the input variables uncertainties. Broadly speaking, the method takes into account the whole alteration and interactions of the input parameters (Saltelli et al., 2004).

GSA is known as one of the reliable sensitivity methods and have been used widely throughout many different fields and studies. One of the main advantages of utilizing GSA is that it considers the effects of uncertain input parameters over the whole input variables, where the interaction between parameters are included (Tian, 2013). On the other hand, more simple methods can be used for less complex or important experiments. There are many known methods of sensitivity, of which some of the most commonly used are discussed below:

- One at a Time Sensitivity Analysis is one of the fundamental methods and commonly known as the simplest method. The procedure can be performed by altering parameters one by one while others remain constant (Hamby, 1994).
- The Sensitivity Index is also known as one of the simplest methods. A sensitivity analysis can be performed by calculating the differences of output percentage by varying an input parameter between its minimum and maximum values. Maximum, D_{max}, and minimum, D_{min}, output values are determined by varying the input parameters over their existing range. The sensitivity index is calculated as shown in Equation 2.1 (Hoffman and Gardner, 1983).

$$SI = \frac{D_{max} - D_{min}}{D_{max}} \tag{2.1}$$

2.1 Factorial Design

Factorial design is known as one of the experimental methods of sensitivity analysis. It is widely utilized within different fields of engineering, particularly when there are several parameters in the model. The results from Zangeneh et al., 2002 studies showed the efficiency of factorial design on geotechnical related problems. Factorial experiments evaluate how multiple independent variables affect one or many dependent variables (Douglas, 2013). The analysis usually considers the number of all parameters and provides runs for the combination of dependent and independent variables (Hamby, 1994).

2.1.1 Two-level Full Factorial Design

There are several types of factorial designs which can be used in research work, but the most comprehensive one that is discussed further is called "K" factors or full factorial design, where low and high levels of each factors are defined. The levels of the factors can be quantitative or qualitative. For instance, qualitative factors are used in this report and it is defined as "high" and "low" levels (Douglas, 2013). The full factorial design provides an experimental analysis which is consisting of a defined level for each factor. The combination of the levels and factors are called treatment combination. The design specifies all combinations of the levels of factors. Hence, to study the effects of "K" factors, 2^k observations are required (Mee, 2009). Also, a full factorial design can reveal the effects of one or several factors on the levels of different factors (Cox, 1958).

2.1.2 Two-level Fractional Factorial Design

Fractional factorial design is utilized to investigate the most critical factors that can affect the results. The approaches are performed by choosing the fraction of the one or two full factorial designs. In these experiments, the number of runs is highly dependent on the number of main factors. As the number of the main factor increases, the number of treatment combinations for the design increase rapidly (Douglas, 2013). Fractional factorial design plays an important role on decreasing the number of runs. This can be done by neglecting of some high-order interactions and obtaining the main effects and low-order interaction by running full factorial design (Douglas, 2013). Moreover, fractional experiments are utilized to reduce the number of the experiments by minimizing the main effects of the factors that might not appoint the combination of the other factors. However, evaluating all parameters and their side combinations might not be interesting in all cases, depending on the study (Gunst and Mason, 2009).

Generally, it is smart to avoid full factorial design due to higher expenses of experimentation. However, in reality each input variables and their interactions might be critical. According to these facts, it would be preferable to implement a smaller experiment to be able to determine the dominant variables and their interactions. Also, randomly assuming the interactions between factors or individual factors might lead to incorrect outputs (Gunst and Mason, 2009). Previous studies might be useful to determine the dominant factors. Some principles toward designing fractional factorial design are discussed under the following headlines.

Aliases

Aliasing are introduced by fraction of full factorial design while considering the factor effects. Aliasing is defined as effecting of two or more factor effects with each-other. For instance, two factor effects are aliased with each-other, if the probability of one effect contains the effects of the other factor effect at the same time. Generally, the aliases refer to the correlation between the factor effects not correlating between response values and input values (Gunst and Mason, 2009).

Main effects

The effect of a primary factor of interest in each experiment is called main effect. It is defined as an alteration in the response of the design which is made by changing the level of the factors which is called effects of a factor (Douglas, 2013). For a 2^k design, the main effects and the h-factor interaction effects can be formulated as below (Box and Hunter, 1961).

k,	main effects
$\frac{k(k-1)}{2!}$,	2-factor interaction effects
$\frac{k(k-1)(k-2)}{3!}$,	3-factor interaction effects
$\frac{k(k-1)(k-2)...(k-1-h)}{h!}$,	h-factor interaction effects

Furthermore, effect of the each parameter for a 2^{k-p} design can be calculated as in Equation 2.2. Where K stands for the number of studied parameters and p stands for the generators where the parameter interactions can be defined.

$$Effect_i = \frac{2(contrast)}{N} \tag{2.2}$$

Where N = 2^{k-p}, which stands for the number of the runs and the contrast can be determined by using the plus and minus sings in each column of the design matrix. Besides, a 2^{k-p}-1 effects and their interactions can be estimated for a 2^{k-p} experiment (Douglas, 2013). Also, screening and projecting a 2^{k-p} design is required to identify the factors with high effects. These procedures can minimize the calculation time.

Resolution

The fractional factorial design can be divided into different types based on their resolutions. The experiment resolution is dependent on the degree of the fractionation of the test, where higher degrees lead to too general assumptions to be able to obtain precise interactions. The meaning of degree of fractionation is the degree of the fractions that is considered, compared to the full factorial design (Box and Hunter, 1961). Generally, researchers tend to have the highest possible resolution, because the highest resolution leads to less confined assumptions. There are three different types of design resolutions as discussed below (Douglas, 2013).

- Design of Resolution III: The main effects are not aliased with each other, but they are aliased with two-factor interactions. Also, two-factor interactions might be aliased with each other.
- Design of Resolution IV: The main effects are not aliased with each other or two-factor interactions, but two-factors can be aliased with each other. Accordingly, the main effects can be estimated for a 2^{k-p} design with a resolution of IV if three or higher factors are eliminated.
- Design of Resolution V: Main effects and two-factor interactions are not confound with any other main effects or two-factor interactions, but two-factor interactions can be aliased with three-factor interactions. The experiments with resolution of V are known as one the powerful designs since it projects all main effects and two factor interactions while neglecting the aliases of three or more factors.

3

Site description

3.1 Case study

The Perniö failure test is a full scale test of an embankment, loaded until failure. The test was conducted on old train tracks near the railway from Helsinki to Turku, near the Finnish city of Perniö. The city is located in the municipality of Salo, south west of Finland where there are highly sensitive soft clays (Mansikkamäki, 2015). For the location of the test, see Figure 3.1.

Figure 3.1: Location of Perniö case study.

3.2 Full scale failure test

In order to carry out the failure test, a 60 m long embankment with a height of 0.6 m and a slope of 1:3 was built on top of the old railway. The load on top of the embankment consisted of four 2.5 m wide containers, which was gradually filled with sand until failure occurred. Several approaches were considered to reduce the stability and to control the slip surface. Therefore, a ditch of 2 m depth was excavated at a distance of 14.5 m from the toe of the embankment. The excavated soil between the embankment and the ditch were placed at the opposite side of the ditch as a counter weight. A photo taken at the test site can be seen in Figure 3.2. Additionally, the groundwater that appeared in the ditch was pumped out to provide a dry condition during the test. Initial calculations indicated that the final slip surface would end at the bottom of the excavated ditch (Mansikkamäki, 2015).

Figure 3.2: Photo taken at the Perniö test site, before failure (Mansikkamäki, 2015).

The site was divided into 6 cross sections, where the cross section D was located between container 2 and 3, as shown in Figure 3.3. The failure occurred at the location of container 2, near the cross-section D (Mansikkamäki, 2015).

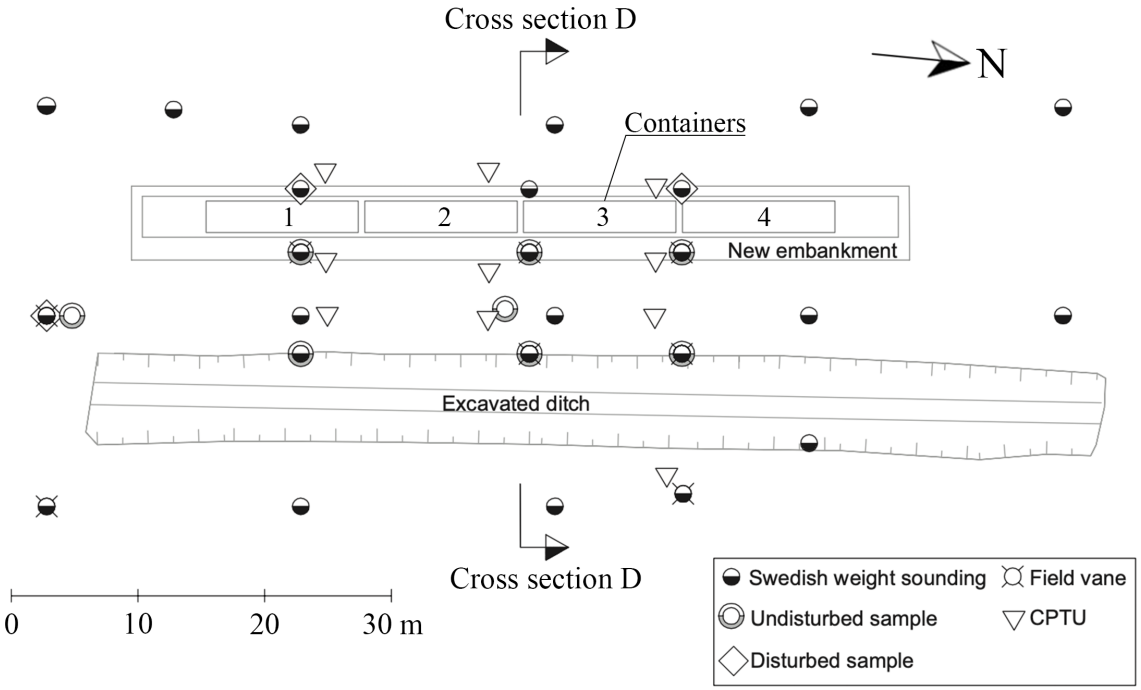

Figure 3.3: Overview, scale of the test embankment and Cross-section D (Mansikkamäki, 2015) (Lehtonen et al., 2015).

The stratigraphy of the site is similar to the typical Finish post-glacial layering. The derived layers of the site can be seen in Figure 3.4. The soil profile of the site, from top to bottom, consists of sand and gravel, which was placed there as fill for the old embankment. Beneath the old fill, the layering was dry crust, soft clay, clayey silt, dense sand and dense moraine (Mansikkamäki, 2015). The old fill layer had a thickness of around 1.5 m and the dry crust around 0.6 to 0.9 m. The soft clay under the dry crust had a thickness varying between 3.5 and 4.5 m, and the clayey silt layer was around 1.5 m thick. The groundwater level was measured to be at 1.3 m below the ground surface during the test (Mansikkamäki, 2015). The soil tests on the site illustrates that the soil layers were not completely horizontal and were increasing in depth towards east (Lehtonen, 2011).

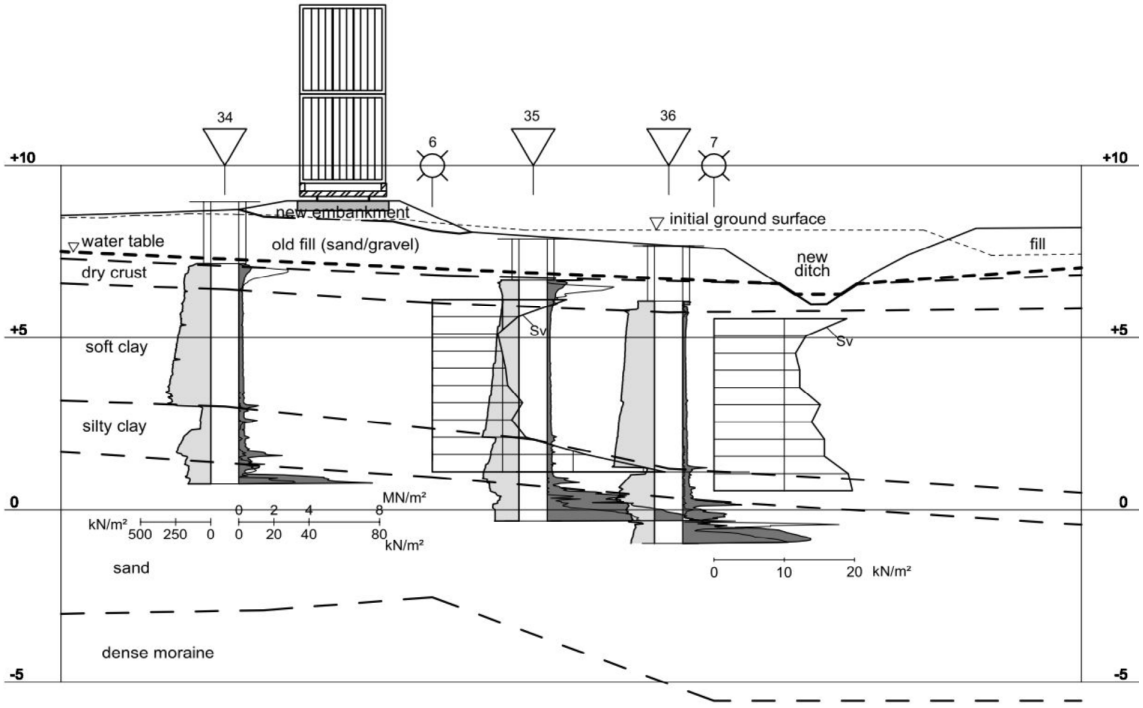

Figure 3.4: Stratigraphy of cross-section D of the Perniö failure test site (Lehtonen et al., 2015).

External loading during failure test

To reach failure of the embankment, the load of the containers was gradually increased by adding sand into the containers. The load steps from each container can be seen in Figure 3.5, and a detailed loading process can be seen in Table A.5, in the Appendix. The final failure of the embankment occurred at the location of the second container, at a load of 87.3 kPa. Due to a width of the load of 2.5 m, the total line load was 218 kN/m at failure (Lehtonen, 2011). A photo taken at the site after the failure can be seen in Figure 3.6.

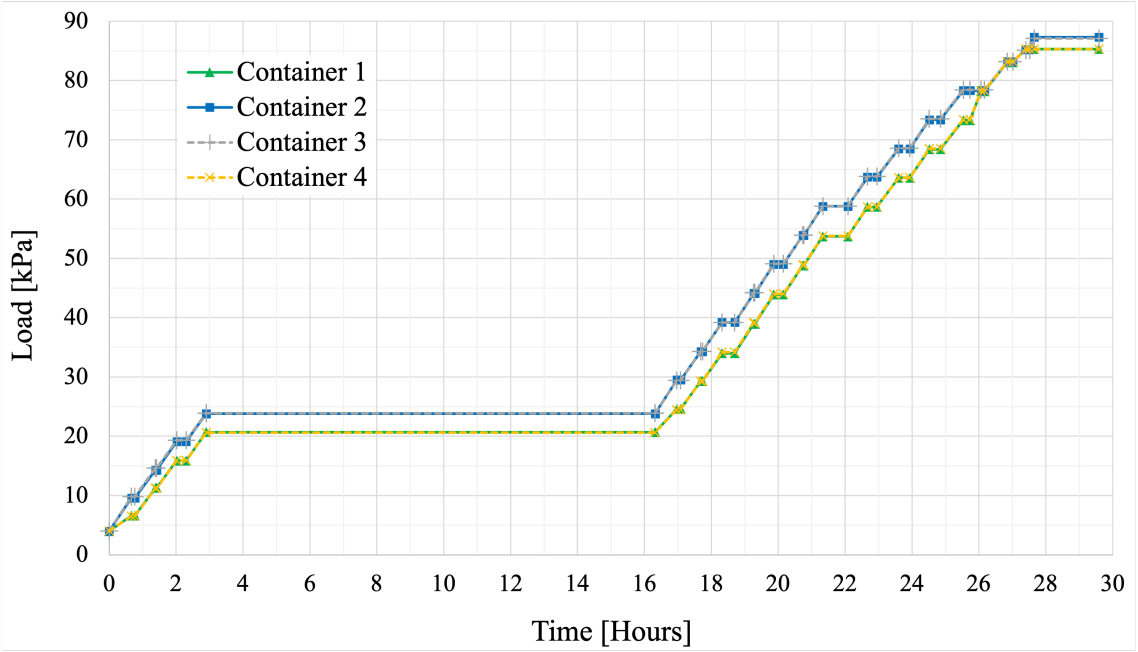

Figure 3.5: Load versus time of the four containers during the Perniö test embankment (Lehtonen, 2011).

Figure 3.6: Photo taken at the site after failure of the embankment (Lehtonen, 2011).

3.3 In-situ sampling and investigation

In-situ sampling and investigations were first implemented in the summer of 2009. 24 Swedish Weight Soundings, 13 Vane Shear Tests, and 10 CPTU tests were conducted before the failure test. The location of the samples and tests, as well as the surrounding area can be seen in Figure 3.7. Also, sampling was done using NGI Ø54 mm, NGI Ø86 mm and Swedish Standard STII 50 mm piston sampler to collect undisturbed samples. Undisturbed samples were collected from 19 different points and disturbed samples were taken form two areas. After the failure test, 8 undisturbed samples were carried out using NGI piston samplers between the test site and the Helsinki-Turku railway, about 40 m away from the failure location. Also, 9 extra CPTU tests were performed after the failure. (Mansikkamäki, 2015).

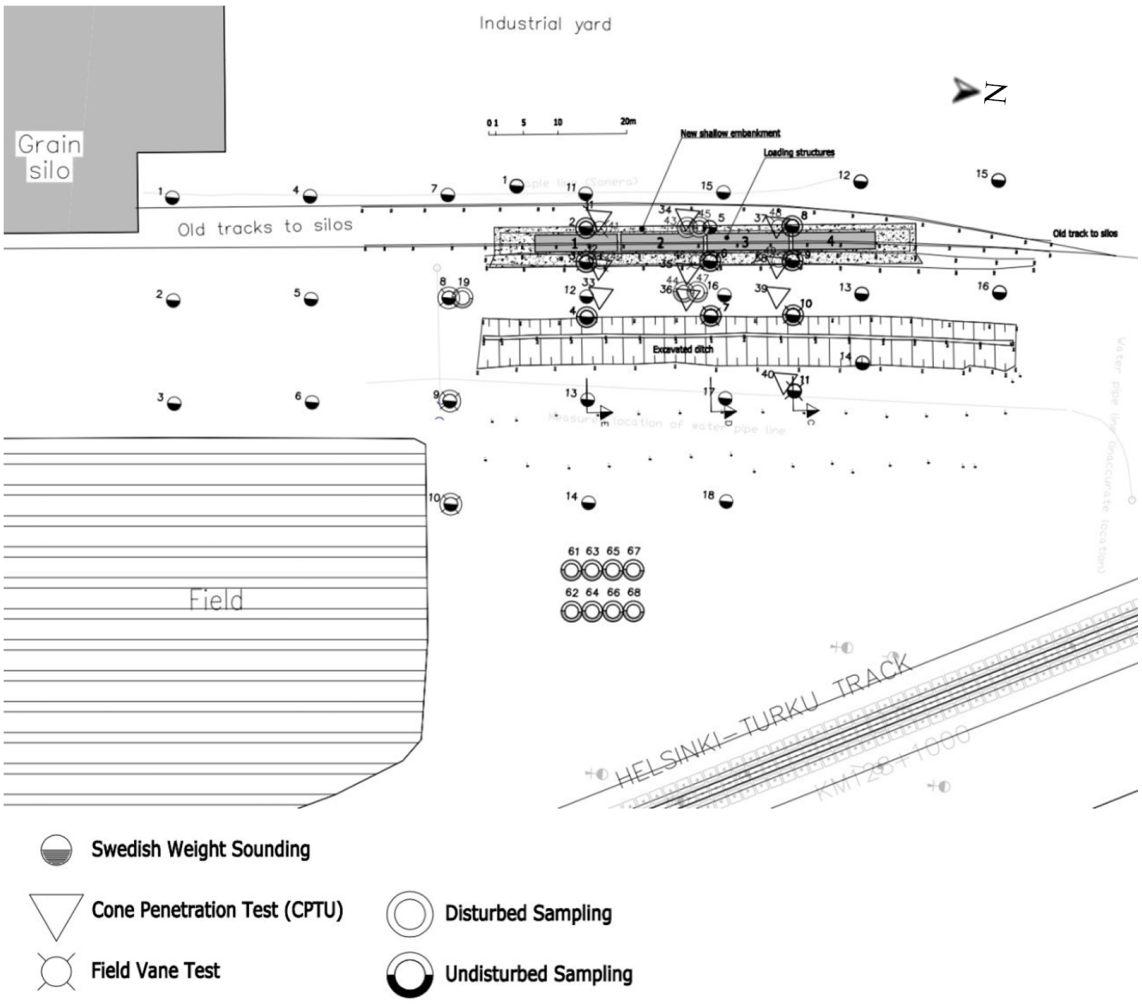

Figure 3.7: The surrounding area, sampling and tests of the site (Mansikkamäki, 2015).

Automatically monitored inclinometers were installed in order to study the horizontal displacements and failure behavior of the soil before the failure. A total of 9 inclinometer tubes in 3 lines were installed laterally alongside the gap between the cars. All inclinometers were placed until the layer of dense sand and moraine

(Lehtonen et al., 2015). Additional settlement tubes were installed between the embankment and the ditch to measure the vertical displacements. The tubes consist of pressure transducers so that, the one side was fixed at certain elevation and the other side moves as soils settle. The tubes were horizontally placed 30 to 50 cm below the embankment crest, toe, and the edge of the ditch (Lehtonen et al., 2015). Also, strain-type pore pressure transducers were utilized to monitor the changes in pore pressure within the slip surface. Thus, 37 strain-type transducers were installed in the cross section between car number 2 and 3 in the depth corresponds to failure slip. A more detailed figure of the instruments can be seen in the Appendix, Figure A.9.

4
Material models

There are many different constitutive models that are able to calculate the behaviour of soils. They all have different degree of simplicity and accuracy, and might also be more suitable to use for different materials. The following subsections will further elaborate the two material models, Mohr-Coulomb and Creep-SCLAY1S, used in the PLAXIS 2D analysis.

4.1 Mohr-Coulomb model

The Mohr-Coulomb model is one of the most well-known models available in PLAXIS 2D. The model is based on linear elastic perfectly-plastic behaviour, where full elastic behaviour is assumed in a linear matter until failure is achieved according to the Mohr-Coulomb failure criterion (Plaxis, 2019b). The deformations after the failure criterion are assumed perfectly-plastic. Mohr-Coulomb models the behaviour of the soil by two bi-linear lines, consisting of an elastic part and a perfectly-plastic part. A schematic figure of an elastic perfectly-plastic model, like Mohr-Coulomb, can be seen in Figure 4.1. It is worth mentioning that the model is not appropriate to use when modelling either normally or over consolidated soft soils (Karstunen and Amavasai, 2017).

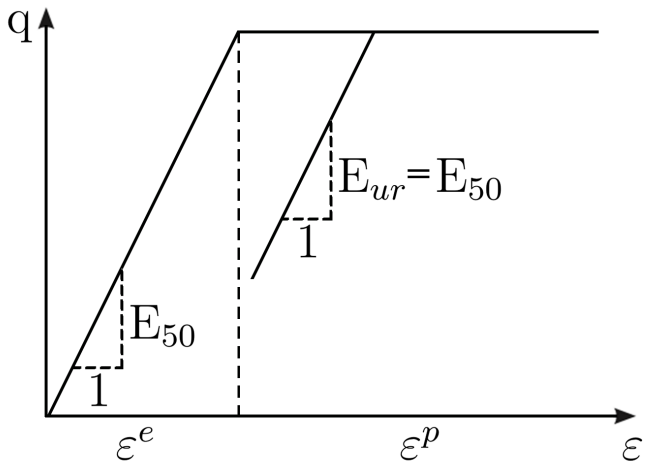

Figure 4.1: Theory of a linear elastic perfectly-plastic model (Plaxis, 2019b).

Within the concept of elasto-plasticity, the strain and strain rates are calculated as can be seen in Equations (4.1) and (4.2), respectively. They are composed of both elastic and plastic parts, which is shown through the superscripts e and p (Plaxis, 2019b).

$$\underline{\varepsilon} = \underline{\varepsilon}^p + \underline{\varepsilon}^e \tag{4.1}$$

$$\dot{\underline{\varepsilon}} = \dot{\underline{\varepsilon}}^p + \dot{\underline{\varepsilon}}^e \tag{4.2}$$

The model is defined within the elastic part through Hooke's law of isotropic elasticity, see equation 4.3. The plastic part is defined through a flow rule, as seen in Equation 4.4 (Plaxis, 2019b).

$$\dot{\underline{\sigma}}' = \underline{\underline{D}}^e \dot{\underline{\varepsilon}}^e \tag{4.3}$$

$$\dot{\underline{\varepsilon}}^p = \lambda \frac{\partial g}{\partial \underline{\sigma}'} \tag{4.4}$$

The assumption of the two bi-linear lines can easily be argued as a significant simplification of the soil behaviour, which can be seen in Figure 4.2 (Tjie-Liong, 2014). Here, it can be seen that during the first half of the E_50 line, the model underestimates the strength, and hence over-estimates the movement. After the point of crossing, the model over-estimates the strength, and under-estimates the movement. Another simplification is that the Mohr-Coulomb model assumes that the unloading-reloading stiffness modulus, E_{ur} is assumed equal to E_{50}. As can be seen from Figure 4.2, the case is often that E_{ur} is more stiff than E_{50}, and the value of E_{ur} is typically 2 to 5 times higher than E_{50}. This might lead to a over-estimation of heaving effects during an unloading scenario (Tjie-Liong, 2014).

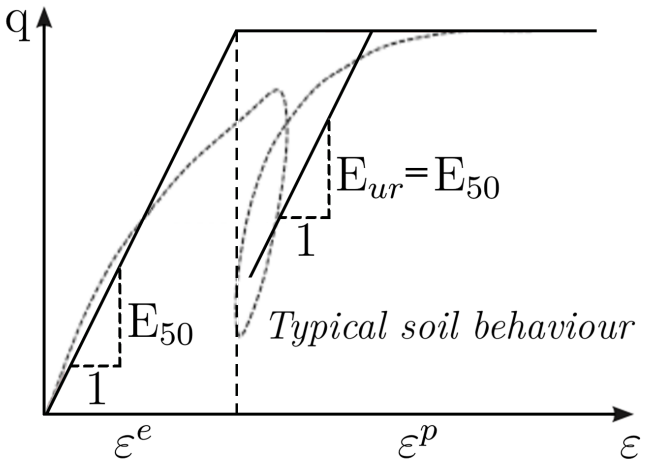

Figure 4.2: Comparison of typical real soil behaviour, and a linear elastic perfectly-plastic model such as Mohr-Coulomb (Tjie-Liong, 2014) (Plaxis, 2019b).

4.1.1 Mohr-Coulomb model parameters

Within the Mohr-Coulomb model, there are several model parameters that need to be evaluated. A full list of the parameters is presented in Table 4.1. Principally, Mohr-Coloumb model is an effective stress model with the effective parameters of E', ν', ϕ' , and c as the effective reference cohesion, c'_{ref}.

Table 4.1: Model parameters used in the Mohr-Coulomb material model with the drainage type set to drained.

Model parameters	**Definition**	***Unit***
E'	Effective Young's modulus	kN/m^2
ν'	Poisson's ratio	-
c'_{ref}	Effective reference cohesion	kN/m^2
ϕ'	Effective friction angle	$^\circ$
ψ	Dilatancy angle	$^\circ$

4.2 The Creep-SCLAY1S model

Creep-SCLAY1S is an advanced model, able to simulate the behavior of soft soils, including mechanisms connected to structure, anisotropic behaviour and rate-dependent events such as creep (Sivasithamparam et al., 2015). Furthermore, the model also takes bonding and destructuration into account. The Creep-SCLAY1S model was first developed in 2014 as a collaboration between Chalmers, NGI and Plaxis bv (Sivasithamparam et al., 2015). The model was included in the PLAXIS 2D/3D CONNECT Edition, update 1, version 20, which was released in January 2020 (van der Sloot, 2020).

In triaxial stress space, the deviatoric stress, q, and the effective stress, p', is calculated by the Equations 4.5 and 4.6. The equations are involving three axes and the subscript letters a and r refers to axial and radial direction, respectively (Sivasithamparam et al., 2015).

$$q = \sigma'_a - \sigma'_r \tag{4.5}$$

$$p' = \frac{\sigma'_a + 2\sigma'_r}{3} \tag{4.6}$$

The model calculates volumetric strain as presented in Equation 4.7, and deviatoric strain is calculated through Equation 4.8 (Sivasithamparam et al., 2015). Furthermore, note that regarding the equations in this Section, the subscript v stands for volumetric strain and q for deviatoric strain.

$$\varepsilon_v = \varepsilon_a + 2\varepsilon_r \tag{4.7}$$

$$\varepsilon_q = \frac{2(\varepsilon_a - \varepsilon_r)}{3} \tag{4.8}$$

Soft soils are often considered to have both elastic and plastic behaviour. The concept of strain, ε, is derived through elasto-viscoplasticity within the Creep-SCLAY1S model, and the total strain is of both elastic parts and creep (viscoplastic), where creep can be considered as inelastic. The equations related the strain rate are hence divided into two parts, the deviatoric and volumetric strain, as can be seen in Equations 4.9 and 4.10 (Sivasithamparam et al., 2015).

$$d\varepsilon_v = d\varepsilon_v^e + d\varepsilon_v^c \tag{4.9}$$

$$d\varepsilon_q = d\varepsilon_q^e + d\varepsilon_q^c \tag{4.10}$$

Both the shear modulus, G, and the bulk modulus, K, are elastic and stress-dependent parameters. They are calculated by Equation 4.11 and 4.12, respectively (Sivasithamparam et al., 2015). Here, ν' is Poisson's ratio, and κ^* is the modified swelling index, which will be further explained in Section 4.2.3.

$$G = \frac{3p'(1-2\nu')}{2\kappa^*(1+\nu')} \tag{4.11}$$

$$K = \frac{p'}{\kappa^*} \tag{4.12}$$

The elastic behavior associated with the Creep-SCLAY1S model is assumed isotropic, with elastic strains connected to the parameters G and K, as presented in Equations 4.13 and 4.14.

$$d\varepsilon_q^e = \frac{dq}{3G} \tag{4.13}$$

$$d\varepsilon_v^e = \frac{dp'}{K} \tag{4.14}$$

For the Creep-SCLAY1S model, creep is defined through the Current Stress Surface, CSS, and the Normal Consolidation Surface, NCS, as shown in Figure 4.3. The model allows creep to take place within the NCS. However, the stress state is allowed outside of the surface due to the fact that the model has no rule of consistency (Sivasithamparam et al., 2015).

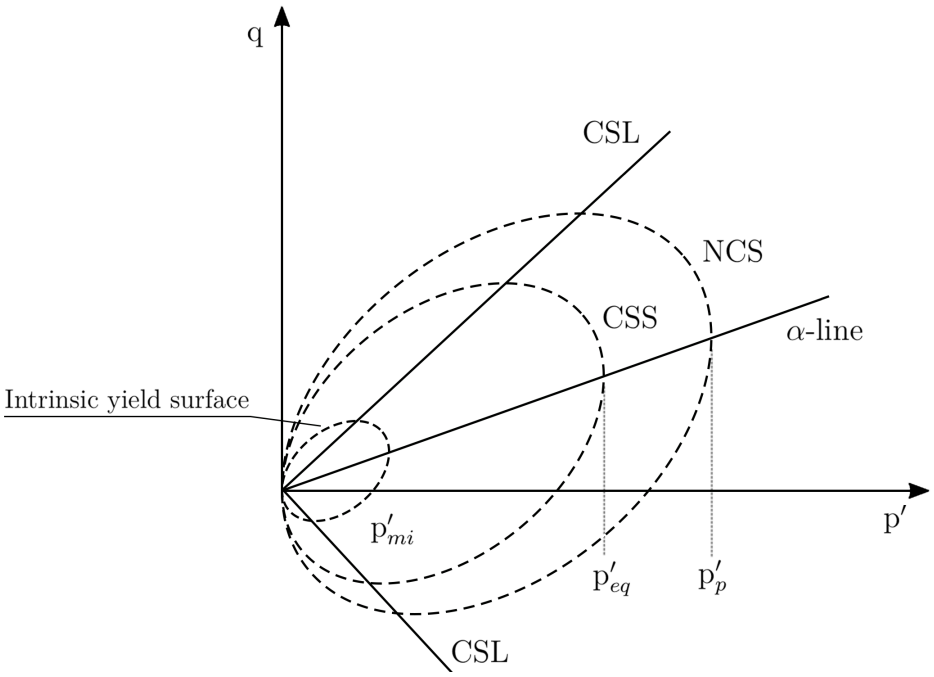

Figure 4.3: CSS, NCS, CSL and the Intrinsic yield surface in a triaxial stress space, as defined in the Creep-SCLAY1S model (Gras et al., 2018).

CSS corresponds to the current state of effective stress. The size and shape of CSS is dependent on p'$_{eq}$ and α, respectively. p'$_{eq}$ is calculated thought Equation 4.15 (Gras et al., 2018).

$$p'_{eq} = p' + \frac{(q - p'\alpha)^2}{p'(M(\theta_\alpha)^2 - \alpha^2)} \tag{4.15}$$

The anisotropic line, α is a scalar that determines the inclination of the CSS and NCS, which can be seen in Figure 4.3. Furthermore, it can be seen from the Figure that the value of α gives the model an anisotropic yield surface. If the yield surface was of isotropic nature, the surface would not have increase of the α line. Creep-SCLAY1S has a law connected to the rotational hardening, which is shown in Equation 4.16, and calculates the slope of the α-line (Laera et al., 2018).

$$d\alpha = \omega \left(\left(\frac{3\eta}{4} - \alpha \right) \langle d\varepsilon_v^c \rangle + \omega_d \left(\frac{\eta}{3} - \alpha \right) |d\varepsilon_q^c| \right) \tag{4.16}$$

Connected to the Creep-SCLAY1S model, there are also two laws regarding hardening behaviour. The size of the NCS is connected to one of the hardening laws, which can be seen in Equation 4.17. The law describes the range of p'$_p$ and hence the size of the NCS. p'$_{p0}$ is the initial isotropic pre-consolidation pressure, and e_v^c is the volumetric creep strain. λ^* and κ^* are explained further in section 4.2.3 (Sivasithamparam et al., 2015).

$$p'_p = p'_{p0} exp \left(\frac{\varepsilon_v^c}{\lambda^* - \kappa^*} \right) \tag{4.17}$$

Equation 4.18 explains the degradation of the bonding parameter χ.

$$d\chi = \xi\chi(|d\varepsilon_v^c| + \xi_d|d\varepsilon_q^c|) \tag{4.18}$$

The stress ratio at critical state, M(θ_α) is dependent on the modified Lode angle, θ_α, M_c and M_e. See Equation 4.19. The model parameters M_c and M_e will be further explained in Section 4.2.5 (Sivasithamparam et al., 2015).

$$M(\theta_\alpha) = M_c\left(\frac{2m^4}{1+m^4+sin3\theta_\alpha(1-m^4)}\right)^{1/4}, \text{ where m} = M_e/M_c \tag{4.19}$$

Equation 4.20 is used to simulate creep. The model parameters τ and μ_i^* are related to creep will be further explained in the Section 4.2.4. Connected to Equation 4.20, $\eta_{K_0^{nc}}$ is calculated through Equation 4.21, and K_0^{nc} is determined using Jaky's formula as presented in Equation 4.22 (Leoni et al., 2008).

$$d\Lambda = \frac{\mu_i^*}{\tau}\left(\frac{p'_{eq}}{p'_p}\right)^\beta\left(\frac{M(\theta_\alpha)^2-\alpha_{K_0^{nc}}^2}{M(\theta_\alpha)^2-\eta_{K_0^{nc}}^2}\right) \tag{4.20}$$

$$\eta_{K_0^{nc}} = \frac{3(1-K_0^{nc})}{1+2K_0^{nc}} \tag{4.21}$$

$$K_0^{nc} = 1 - sin\phi' \tag{4.22}$$

β is calculated through Equation 4.23 (Sivasithamparam et al., 2015).

$$\beta = \frac{\lambda_i^* - \kappa^*}{\mu_i^*} \tag{4.23}$$

An associated flow rule connected to the model can be seen in Equations 4.24 and 4.25, which calculates the creep strain rate (Sivasithamparam et al., 2015).

$$d\varepsilon_v^c = d\Lambda\frac{\partial p'_{eq}}{\partial p'} \tag{4.24}$$

$$d\varepsilon_q^c = d\Lambda\frac{\partial p'_{eq}}{\partial q} \tag{4.25}$$

4.2.1 Creep-SCLAY1S model parameters

For the full list of model parameters within the Creep-SCLAY1S model, see Table 4.2. In the following subsections, 4.2.2 to 4.2.7, the model parameters will be further explained.

Table 4.2: Model parameters used in the Creep-SCLAY1S material model.

Parameter	Definition	*Unit*
κ^*	Modified swelling index	-
λ_i^*	Modified intrinsic compression index	-
ν'_{ur}	Poisson's ratio for unloading-reloading	-
M_c	Slope of critical state line in compression	-
M_e	Slope of critical state line in extension	-
μ_i^*	Intrinsic modified creep index	-
τ	Reference time	*Time*
ω	Absolute effectiveness of rotational hardening	-
ω_d	Relative deviatoric effectiveness of rotational hardening	-
ξ	Absolute rate of destructuration	-
ξ_d	Relative rate of destructuration	-
POP	Pre-overburden pressure	*kPa*
OCR	Overconsolidation ratio	-
χ_0	Initial bonding	-
α_0	Initial anisotropy	-

4.2.2 Initial state parameters

The initial state parameters used to initialise the size of NCS are POP or OCR. OCR is defined as the quotient between the effective pre-consolidation pressure and the effective vertical stress, and POP as the difference, see Equations 4.26 and 4.27. Within the Creep-SCLAY1S model, either one of the two model parameters should be used.

$$OCR = \frac{\sigma'_{pc}}{\sigma'_v} \tag{4.26}$$

$$POP = \sigma'_{pc} - \sigma'_v \tag{4.27}$$

4.2.3 Parameters related to isotropic stiffness

The parameters related to isotropic stiffness and compressibility are the modified intrinsic compression index, λ_i^*, the modified swelling index, κ^*, and Poisson's ratio for unloading-reloading, ν'_{ur}. The model parameters λ_i^* and κ^* are derived as the slope of the intrinsic compression line, and the elastic swelling line of the stress-strain curve, respectively. For an illustration of deriving the two parameters, see Figure 4.4. Both λ_i^* and κ^* are unitless. A common ratio between λ_i^* and κ^* is that λ_i^* is somewhere between 2.5 and 7 times larger than κ^*. The values are derived according to equations 4.28 and 4.29 (Laera et al., 2018).

$$\lambda_i^* = \frac{\lambda_i}{1 + e_0} \tag{4.28}$$

$$\kappa^* = \frac{\kappa}{1 + e_0} \tag{4.29}$$

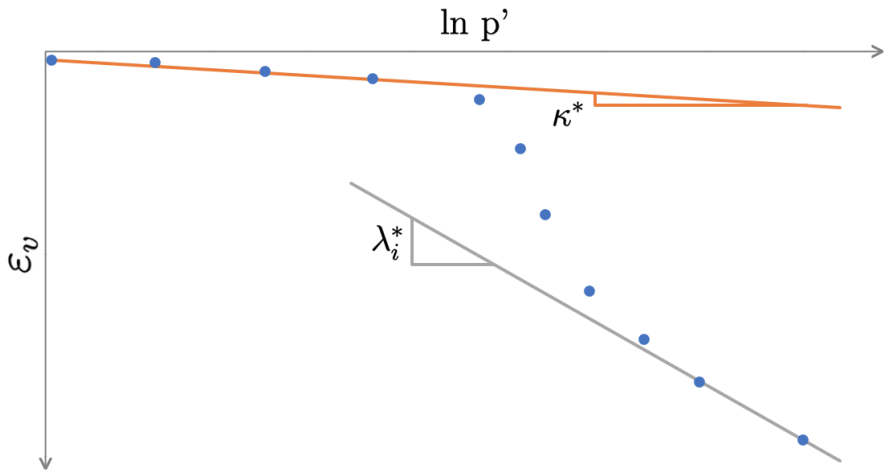

Figure 4.4: Deriving of λ_i^* and κ^* from a ln p', ε_v plane plot (Gras et al., 2018).

Poisson's ratio for unloading-reloading, ν'_{ur}, is a elastic parameter connected to isotropic stiffness. For soft soils, a reasonable value range can be considered between 0.1 and 0.2. For geotechnical related problems where horizontal stresses have a significant impact, it is recommended to conduct a sensitivity study on ν'_{ur} (Karstunen and Amavasai, 2017).

4.2.4 Parameters related to creep

There are two parameters related to creep, the modified intrinsic creep index, μ_i^*, and the reference time, τ. They are both used to describe the creep strain rates. μ_i^* is derived according to Figure 4.5 (Karstunen and Amavasai, 2017), and τ is set according to the time frame of the incremental loading oedometer test, IL OT, used to determine the POP or OCR (Sivasithamparam et al., 2015).

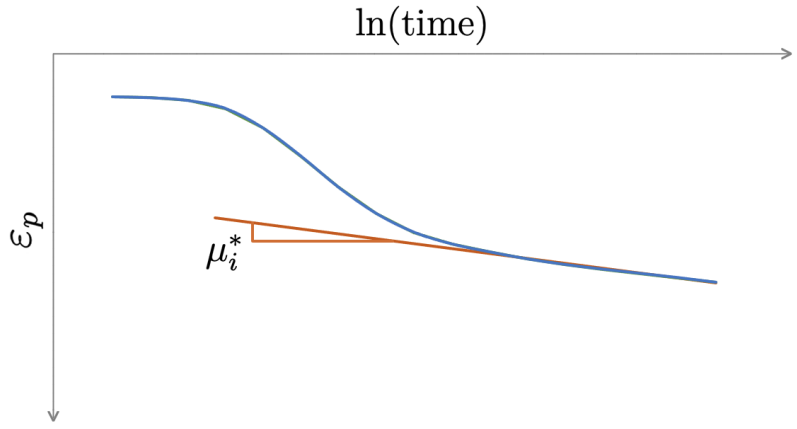

Figure 4.5: Deriving of μ_i^* from a ln(time), ε_p plane plot (Sivasithamparam et al., 2015).

4.2.5 Parameters related to critical state

The two parameters related to critical state are M_c and M_e, which can be defined as the slope of the critical state line through undrained triaxial tests in compression and extension, respectively (Sivasithamparam et al., 2015). In the Equations 4.30 and 4.31, which can be used to assumed the two parameters, ϕ'_c and ϕ'_e are the critical state friction angle in compression and extension, respectively (Laera et al., 2018).

$$M_c = \frac{6sin\phi'_c}{3 - sin\phi'_c} \tag{4.30}$$

$$M_e = \frac{6sin\phi'_e}{3 + sin\phi'_e} \tag{4.31}$$

Compression and extension are fundamental loading paths involved in geotechnics. For embankment stability these idealised loading paths are interpreted to occur in the soil at different locations along the failure plane Figure 4.6 (Dijkstra, 2019a).

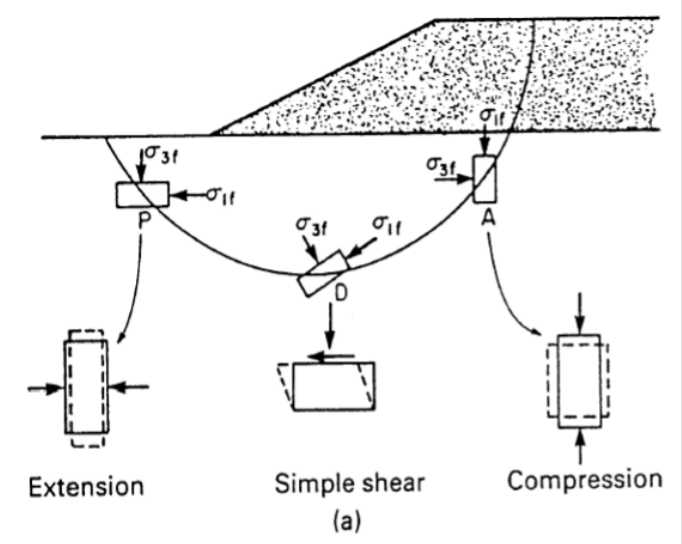

Figure 4.6: Compression, simple shear and extension in a slope stability related problem (Dijkstra, 2019a).

4.2.6 Parameters related to anisotropy

The parameters related to anisotropy are α_0, ω and ω_d. The initial anisotropy, α_0, is calculated using Equation 4.32 (Wheeler et al., 2003). Here, $\eta_{K_0^{nc}}$ is calculated through Equation 4.21, and K_0^{nc} according to Jaky's formula as can be seen in Equation 4.22.

$$\alpha_0 = \alpha_{K_0^{nc}} = \frac{\eta^2_{K_0^{nc}} + 3\eta_{K_0^{nc}} - M_c^2}{3} \tag{4.32}$$

The absolute effectiveness of rotational hardening, ω, can be calculated by the Equation 4.33 (Leoni et al., 2008), with reasonable bounds according to the simplified Equation 4.34 (Laera et al., 2018).

$$\omega = \frac{1}{\lambda^*} ln \left(\frac{10M_c^2 - 2\alpha_0\omega_d}{M_c^2 - 2\alpha_0\omega_d} \right) \tag{4.33}$$

$$0 < \omega \leq \frac{2.9}{\xi_i^* ln \left(\frac{4(1+\chi_0)}{2+\chi_0} \right)} \tag{4.34}$$

Note that ξ_i^* is calculated as shown in Equation 4.35 (Gras et al., 2018).

$$\xi_i^* = \lambda_i^* - \kappa^* \tag{4.35}$$

The relative deviatoric effectiveness of rotational hardening, ω_d, is calculated by using Equation 4.36 (Wheeler et al., 2003).

$$\omega_d = \frac{3\left(4M_c^2 - 4\eta_{K_0^{nc}}^2 - 3\eta_{K_0^{nc}}\right)}{8\left(-M_c^2 + \eta_{K_0^{nc}}^2 - 2\eta_{K_0^{nc}}\right)} \tag{4.36}$$

4.2.7 Parameters related to bonding

The parameters that consider structure and apparent bonding of sensitive clays are the initial amount of bonding, χ_0, the absolute rate of destructuraion, ξ, and the relative rate of destructuraion, ξ_d (Mansikkamäki, 2015).

χ_0 can be derived from experimental testing. However, this needs to be done accurately since the method is highly sensitive to the quality of laboratory tests. Another approach is to calculate χ_0 based on the sensitivity of the material, see Equation 4.37 (Gras et al., 2017).

$$\chi_0 = S_t - 1 \tag{4.37}$$

There is no experimental procedure to calculate the parameters ξ and ξ_d. Furthermore, optimization and calibration are needed, and hence appropriate ranges are required for both destructuraion parameters. The possible range for ξ_d is between 0 and 1 and a reasonable range in Scandinavian soft clays is between 0.2 and 0.4 (Gras et al., 2018).

ξ can be derived by curve fitting or by calculating upper and lower bounds. Equations for the lower and upper bounds can be seen in Equation 4.38. The upper bound of ξ is highly depending on ξ_d. However, small changes can be seen in the value of ξ when χ_0 is larger than 10 (Gras et al., 2018).

$$\frac{ln2}{\left[ln(2+2\chi_0) - ln\left(1+\frac{\chi_0}{2}\right)\right](1+\xi_d)\xi_i^*} \leq \xi \leq \frac{1+\chi_0}{\xi_i^*\chi_0\left(1+2\xi_d\frac{\alpha_{K_0^{nc}}}{M_e^2}\right)} \tag{4.38}$$

4.3 Soil properties connected to Mohr-Coulomb and Creep-SCLAY1S

For a full list of the soil properties connected to the Mohr-Coulomb and Creep-SCLAY1S models, see Table 4.3. The coefficient of lateral earth pressure in x and z direction, K_0, is defined as the quotient between the horizontal and vertical principal effective stresses. Furthermore, K_0 can be calculated through a modified version of Jaky's Formula, which can be seen in Equation 4.39. In this case, $K_{0,x}$ and $K_{0,z}$ are assumed to be equal.

$$K_0 = (1 - sin\phi')\sqrt{OCR} \tag{4.39}$$

Table 4.3: Soil properties connected to Mohr-Coulomb and Creep-SCLAY1S.

Soil properties	**Definition**	***Unit***
$K_{0,x}$	Coefficient of lateral earth pressure in x direction	-
$K_{0,z}$	Coefficient of lateral earth pressure in z direction	-
γ_{unsat}	Unsaturated unit weight	kN/m^3
γ_{sat}	Saturated unit weight	kN/m^3
e_0	Initial void ratio	-
K_x	Horizontal hydraulic conductivity	m/day
K_y	Vertical hydraulic conductivity	m/day
C_k	Change of permeability	-

5

Numerical model

5.1 Sample quality

The model parameters used in the Creep-SCLAY1S model were derived from both triaxial tests and Incremental Loading oedometer tests, IL OT. The two test methods will be further explained in subsections 5.2 and 5.3. A good sample quality is of utmost importance when it comes to geotechnical related problems. There are many ways to determine the quality of a sample (Carlsten and Henriksson, 1994). Variables such as vertical strain and initial water content can be used for sample quality identification (Lunne et al., 1997). Assessments of the sample quality can also be evaluated based on the $\Delta e/e_0$ criterion, as proposed by Lunne et al., 1997. The basis of the grading system is to compare the change of void ratio when the sample is under the previous effective overburden pressure, as the sample would have experience before being extracted. The method was initially tested on soft low plastic Norwegian clay (Lunne et al., 1997), but is also applicable for sensitive soft clays such as at the test site (Mansikkamäki, 2015).

The evaluation system to grade samples used in this report was according to the $\Delta e/e_0$ criterion, as presented by Lunne et al., 1997. The criterion divides the samples into four categories based on their quality. The categories are very poor, poor, good to fair and excellent. Only 13 samples of IL OT performed using 24 hour load steps were considered good to fair sample quality, and were hence used for this report. No samples showed excellent sample quality (Mataić et al., 2016). The sample quality grading intervals can be seen in Table 5.1 (Lunne et al., 1997). A graph showing the different results of $\Delta e/e_0$ for each sample can be seen in Appendix A.3.

Table 5.1: Sample quality according to the $\Delta e/e_0$ criterion (Lunne et al., 1997).

$\Delta e/e_0$	**Grade**
< 0.04	Excellent
0.04 - 0.07	Good to fair
0.07 - 0.14	Poor
> 0.14	Very poor

5.2 Triaxial tests

In a triaxial test a soil sample is tested under a confining stress (cell pressure), a deviatoric load is applied in the sample by incresing the axial load. The difference between the horizontal and vertical (total or effective) stress is called the deviatoric stress, $\Delta\sigma$ (Craig and Knappett, 2012). If the drainage valve is open during the shearing stage, then the test has a drained loading (D), and if closed, undrained loading (U). Furthermore, depending on the stress state prior to the shearing stage, triaxial tests are often divided into three different main test types. These are unconsolidated-undrained (UU), consolidated-drained (CD), and consolidated-undrained (CU) (Dijkstra, 2019b).

The CU test types can be further divided into three main subcategories (Dijkstra, 2019b):

- Consolidated anisotropic undrained compression (CAUC)
- Consolidated anisotropic undrained extension (CAUE)
- Consolidated isotropic undrained (CIU)

There were two main types of triaxial tests performed at the Perniö test site, CAUC and CAD (anisotropically consolidated-drained). There was a total of 44 CAUC tests and 48 CAD performed (Mataić et al., 2016).

5.3 Incremental loading oedometer tests

During a IL OT, the soil sample is placed under a stepwise increasing vertical load, doubling the load at each stage. The sample is typically a thin slice and the most common test is done during a 24 hour period. After the loading stages, an unloading phase is introduced. For the Perniö test location, a total of 75 IL OT were performed on the clay at different depths. A total of 63 tests were performed during a 24 hours period, and 12 tests were long duration IL OT, performed during 10 or 14 days (Mataić et al., 2016).

5.4 Creep-SCLAY1S model parameter determination

This section will provide information regarding the model parameters obtained for the clay layer, which was modelled using the Creep-SCLAY1S model. The drainage type for the clay layer chosen was the Undrained (A) condition (consolidation). The values of the model parameters used in this report were derived from different data and sources, which will be further explained in this section. A full list of the parameters and their derived values can be seen in Table 5.2.

5.4.1 Initial state parameters

The pre-overburden pressure, POP, was used in the PLAXIS 2D model, meanwhile OCR was set to 1. POP was used instead of OCR since the data fitted better with depth. The derived value for POP was calculated as 19 kPa, which was the mean value for all of the samples used. The scatter of POP was noteworthy and ranged between 15 and 26 kPa. There was however no clear trend depending on the depth of the samples. POP, plotted versus depth can be seen in the Appendix, Figure A.7.

5.4.2 Parameters related to isotropic stiffness

λ_i^* and κ^* were derived from the IL OT, provided by Mataić et al., 2016. The values of λ_i^* and κ^* were chosen according to the mean value of the samples used. The different values of λ_i^* and κ^* from the samples used can be seen in Appendix A, Figure A.3 and Figure A.4. λ_i^* was derived to be 0.076 and κ^* as 0.027.

The derived values of λ_i^* and κ^* were then tested versus a axial stress-specific volume plot from the IL OT. Here, only the tests with approved sample quality were plotted. The axial stress has been plotted as a function of the natural logarithm. The calculation process of λ_i^* and κ^* has hence taken this into account. The graph showed a clear fit for both λ_i^* and κ^*, which can be seen in Figure 5.1.

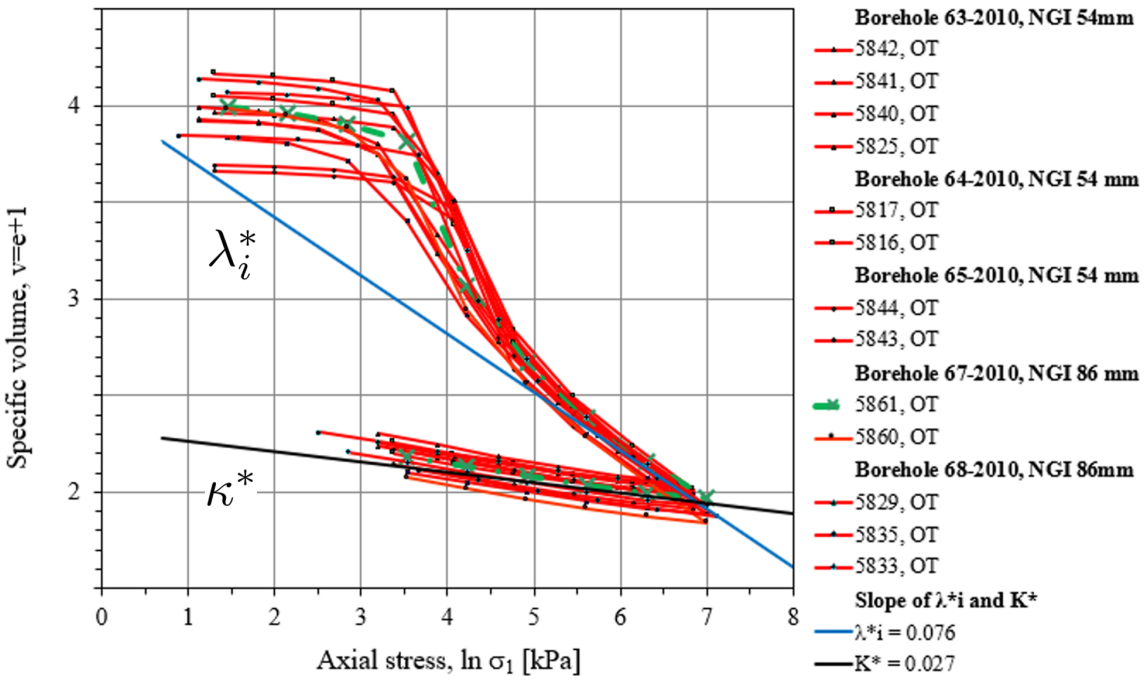

Figure 5.1: Graph of λ_i^* and κ^* derived from the IL OT of Perniö clay (Mataić et al., 2016).

As discussed in Section 4.2.3, a reasonable range of ν'_{ur} for soft soils can be considered to be between 0.1 and 0.2 (Karstunen and Amavasai, 2017). Therefore, the value was set to 0.15 as the original value.

5.4.3 Parameters related to creep

The model parameter μ_i^* was derived from the works of Mataić et al., 2016. The scatter of the calculated values of μ_i^* from each sample can be seen in Appendix A, Figure A.5. The value chosen for the original calibration was the mean value of the samples used, which was equal to 2.6E-3.

The reference time, τ, in the PLAXIS 2D model was set to the unit of days, and the parameter was set to 1 day. This is because IL oedometer tests with 24 h load steps were used to determine POP.

5.4.4 Parameters related to critical state

M_c and M_e were calculated through the Equations 4.30 and 4.31, respectively. According to the works of Mataić et al., 2016, the critical state friction angle in compression and extension were both equal to 34.6 °. Hence, the calculated value for M_c was 1.40, and M_e was 0.95.

5.4.5 Parameters related to anisotropy

The initial anisotropy, α_0, was calculated to 0.54 through Equation 4.32. The value was derived by calculating K_0^{nc} to 0.43, according to Jaky's Formula in Equation 4.22, with a friction angle of 34.6 °. $\eta_{K_0^{nc}}$ was calculated to 0.914 according to Equation 4.21.

The relative deviatoric effectiveness of rotational hardening, ω_d, was calculated to 0.94, by using Equation 4.36. The absolute effectiveness of rotational hardening, ω, was derived from the works of Mataić et al., 2016, and set to the value of 51.9. The different values of ω from each sample can be seen in the Appendix, Figure A.6, where the mean value of the samples was chosen for the original calibration. According to Equation 4.34, the upper bound was calculated to be 102. Hence, this could validate the value of 51.9 since it is between 0 and 102.

5.4.6 Parameters related to bonding

χ_0 was calculated to 38, by using Equation 4.37 with a S_t value of 39, as presented by Mataić et al., 2016. Mataić et al., 2016 also concluded the value for ξ_d which was set equal to 0.2. ξ was then derived by calculating the upper and lower bound, according to Equation 4.38. The upper bound was calculated to 16.9, and the lower bound to 8.7. The results can be seen in Figure 5.2, where the value of ξ is dependent on ξ_d. The mean value of 15.3 was chosen for ξ as the original parameter.

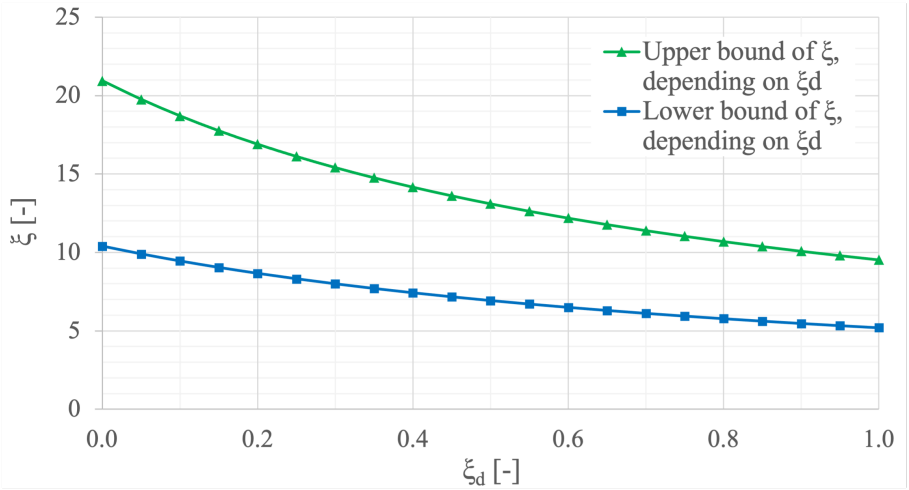

Figure 5.2: Upper and lower bound of ξ depending on ξ_d, as calculated with $\chi_0 = 38$, $\xi_i^* = 0.049$, $\alpha_0 = 0.54$, Me $= 0.95$.

5.4.7 Final values of the Creep-SCLAY1S model parameters

In Table 5.2, the final values used as the original Creep-SCLAY1S model parameters are shown. These were the values with which the model initially was run, and from where the lower and upper bounds originate from within the Global Sensitivity Analysis.

Table 5.2: The Creep-SCLAY1S model parameters used for the initial analysis, before variation. The drainage type was set to Undrained (A).

	Clay layer	***Unit***
Model parameters		
κ^*	0.027	-
λ_i^*	0.076	-
ν'_{ur}	0.15	-
M_c	1.4	-
M_e	0.95	-
μ_i^*	2.6E-3	-
τ	1	*Days*
ω	51.9	-
ω_d	0.94	-
ξ	12.8	-
ξ_d	0.2	-
POP	19	*kPa*
χ_0	38	-
α_0	0.54	-

5.5 Mohr-Coulomb model parameters

The Mohr-Coulomb material model was used to model the behaviour of the embankment, fill, dry crust and moraine. For all these layers, drained condition will be used. The model parameters were gathered from Mansikkamäki, 2015 and Mataić et al., 2016, as well as reasonable and typical values from Karlsson and Moritz, 2016.

The Young's modulus, E', was set to between 10 and 40 MPa for the different layers. Poisson's ratio was assumed to be between 0.3 and 0.35. The effective reference cohesion was set between 0.2 and 5 kN/m^2. The effective friction angle was set to between 33 and 36°, and the dilatancy angle was set to 0° for all layers. The full list of the Mohr-Coulomb model parameters can be seen in Table 5.3.

Table 5.3: The parameters used for the layers modeled with Mohr-Coulomb. Drainage type Drained was set for all of these layers.

	Embankment	**Fill**	**Dry crust**	**Moraine**	***Unit***
Model parameters					
E'	40 000	30 000	10 000	20 000	kPa
ν'	0.3	0.3	0.35	0.35	-
c'_{ref}	5	5	3	0.2	kN/m^2
ϕ'	35	33	35	36	°
ψ	0	0	0	0	°

5.6 Additional soil properties

The soil properties were chosen according to in-situ investigation of the Perniö site, as well as reasonable values according to literature. The saturated and unsaturated unit weights were set to 14.1 kN/m^3 for the clay layer, according to Mataić et al., 2016, and the rest were assumed between 17 and 21 kN/m^3, according to Karlsson and Moritz, 2016. For the clay layer, e_0 is set to 2.97 according to Mataić et al., 2016. The different values for e_0 for each sample with good sample quality can be seen in Figure A.2 in the Appendix. Furthermore, e_0 is assumed to be 0.5 for the rest of the layers. $K_{0,x}$ and $K_{0,z}$ were assumed equal, and set for the clay layer according to Section 4.3. For the other layers, $K_{0,x}$ and $K_{0,z}$ were assumed to 0.5.

The data sets related to groundwater were selected as USDA for all layers, with the Van Genuchten hydraulic model. The different grain distributions can be seen in Table 5.4. The horizontal and vertical hydraulic conductivity, K_x and K_y, were set to 2E-5 and 1E-5 m/day respectively, for the clay layer. The assumed difference in horizontal and vertical direction are due to foliation, which typically increase the horizontal hydraulic conductivity. For the rest of the layers, values between 1 and 100 m/day were chosen. The values were set according to the literature values proposed by Fetter, 2018. According to the Plaxis, 2019a, the change of permeability, C_k, is recommended to use when modelling with the following four material models; Soft

soil, Soft soil creep, Hardening soil and Hardening soil with small-strain stiffness. It should otherwise be set to the value of 10E+15, which is the default value set in PLAXIS 2D (Plaxis, 2019a).

Table 5.4: The values of the soil properties used in the model.

	Clay	**Embankment**	**Fill**	**Dry crust**	**Moraine**	***Unit***
General						
γ_{unsat}	14.1	21	19	17	19	kN/m^3
γ_{sat}	14.1	21	19	17	19	kN/m^3
e_0	2.97	0.5	0.5	0.5	0.5	-
Initial						
$K_{0,x}$	0.52	0.5	0.5	0.5	0.5	-
$K_{0,z}$	0.52	0.5	0.5	0.5	0.5	-
Groundwater						
Data set	USDA	USDA	USDA	USDA	USDA	
Type	Clay	Sand	Sand	Sand	Sand	
< 2 μm	70	4	4	4	4	%
2 μm - 50 μm	13	4	4	4	4	%
50 μm - 2 mm	17	92	92	92	92	%
K_x	2E-5	100	20	1	1	m/day
K_y	1E-5	100	20	1	1	m/day
$-\psi_{unsat}$	10E+3	10E+3	10E+3	10E+3	10E+3	m
C_k	10E+15	10E+15	10E+15	10E+15	10E+15	-

5.7 The PLAXIS 2D Model

5.7.1 Geometry

The model geometry was assumed as according to the cross-section D, between container 2 and 3, as seen in Figure 3.3. The geometry of cross-section was presented by Mansikkamäki, 2015 and Lehtonen, 2011. Figure 5.3 illustrates the final geometry of the model. Furthermore, the boundaries were set to a total width of 7 m towards the left side of Figure 5.3, and 12 m to the right side. Figures of the change in geometry from the initial phase to loading of the embankment can be seen in Figure A.5, in the Appendix.

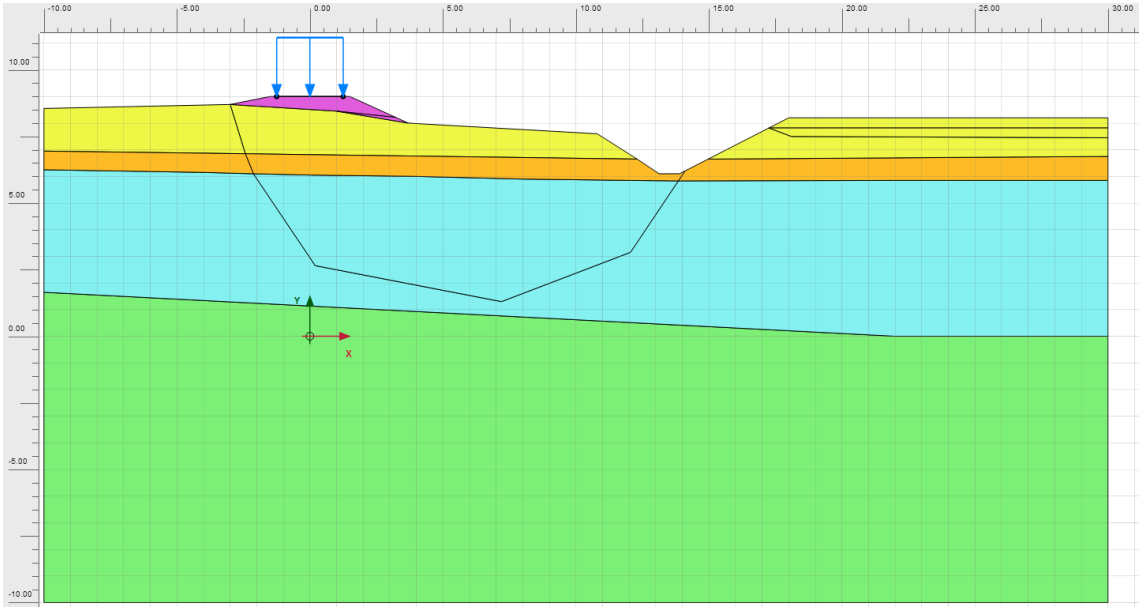

Figure 5.3: Model geometry. Layers from top to bottom; embankment (purple), old fill (yellow), dry crust (orange), clay (blue), moraine (green).

The groundwater flow boundary conditions were defined based on site conditions. The right and left boundaries were set to open because horizontal water flow were expected. The groundwater was modelled in three different ways. For phase 1, the groundwater was set to be 0.2 m above the dry crust. When the excavation was built, the ground water was modelled to decrease from 0.2 m above the dry crust at X_{min} and X_{max}, and then lowered until the excavation. During the loading phases, the water was pumped out from the excavation, which was modelled by a lowering groundwater table during these phases.

The boundary conditions regarding deformations were set to normally fixed on the sides, X_{min} and X_{max}. For a rectangular geometry, this setting allows for vertical deformations, but not horizontal. For the top, the free condition was selected, allowing free deformations. Fully fixed was set at the bottom, allowing no deformations.

Table 5.5: Model conditions.

	$\mathbf{X}_{min}$	$\mathbf{X}_{max}$	$\mathbf{Y}_{min}$	$\mathbf{Y}_{max}$
Deformations	Normally fixed	Normally fixed	Fully fixed	Free
Groundwater flow	Open	Open	Open	Open

5.7.2 Mesh

An evaluation of the mesh quality was conducted to see how sensitive the model was to the mesh settings. As a result, all the mesh settings show virtually identical outcome during the failure phase. Thus it was decided to implement fine mesh for fractional factorial design in order to reduce the time taken to run the model. In contrast, very fine mesh quality was designed for full factorial design to minimize

the possible errors since the full factorials is considered as the most sensitive stage of the study. Additionally, 15-noded elements were set for the PLAXIS 2D model to have higher precision. Moreover, for precise results it was decided to add extra mesh refinement in the areas where the results converges. Thus, a higher element distribution of the area of the slip surface was used. To do that, an extra lines with a safe distance outside of the slip surface were added, to ensure that the mechanisms were not affected by the mesh quality. The areas containing the slip surface and the embankment were refined two times. Figure 5.4 shows the final mesh quality of the model. The number of elements generated were 3471, with a total of 28099 nodes.

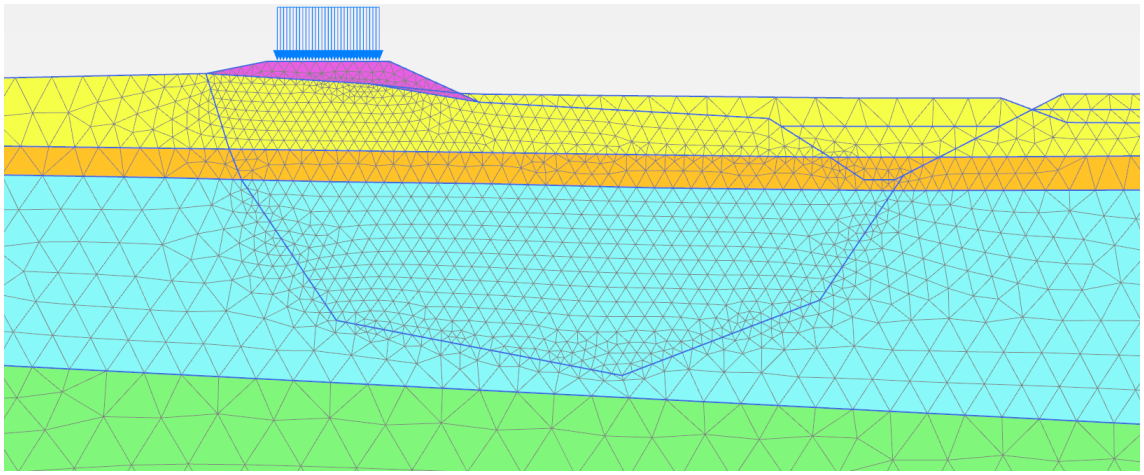

Figure 5.4: Mesh refinement.

5.7.3 Construction stages

In summary, the model consists of an initial phase, four consolidation stages of staged construction, and then additional phases where the load of the containers were increased.

The initial phase was set to the calculation type of K0-procedure, and loading type was set as a staged construction. After the initial phase, the model was made by a total of 70 phases. Phase 1 to 4 were the phases to construct the geometry used for the failure test. Information about the construction-phases can be seen in Table 5.6. The change in geometry is also displayed in the Appendix, Figure A.10. In phase 1 the old fill was applied on top of the dry crust with 5000 days or nearly 14 years assigned for consolidation. The phases 2-5 are illustrating the construction process including building the embankment and digging the ditch. About 10 weeks were spent on excavating the trench and building the new embankment (Lehtonen et al., 2015).

Table 5.6: Description of phase 1 to 4.

	Description	Time
Phase 1	The rest of the old fill was applied	14 years
Phase 2	Half of the ditch was built	3.5 days
Phase 3	The other half of the ditch was built	3.5 days
Phase 4	The embankment was built	9 weeks

Phase 5 to 70 are consolidation stages to increase the line load used to simulate the load from the containers. The line load at phase 5 started at 4 kPa, and was then increased by 5 kPa at a time until phase 13, at a load of 44 kPa. After phase 13, the load was increased by 2 kPa. The model was made by increasing the load at each stage by even values, similar to the Perniö failure test, but with even loads and time, which could give some deviations when compared to the field test. This is due to the fact that the difference in load and time on each step would be another parameter that would affect the results. The steps were divided into larger and smaller steps, where the larger steps were used in the earlier phases, where failure did not occur. The smaller steps were used to get a more exact and accurate results. The larger steps (phase 5 to 12) were set to 58 minutes. The smaller steps (phase 13 to 70) were set to 23.2 minutes, to account for the change of 5 kPa per step to 2 kPa per step. The load versus the consolidation time can be seen in Figure 5.5.

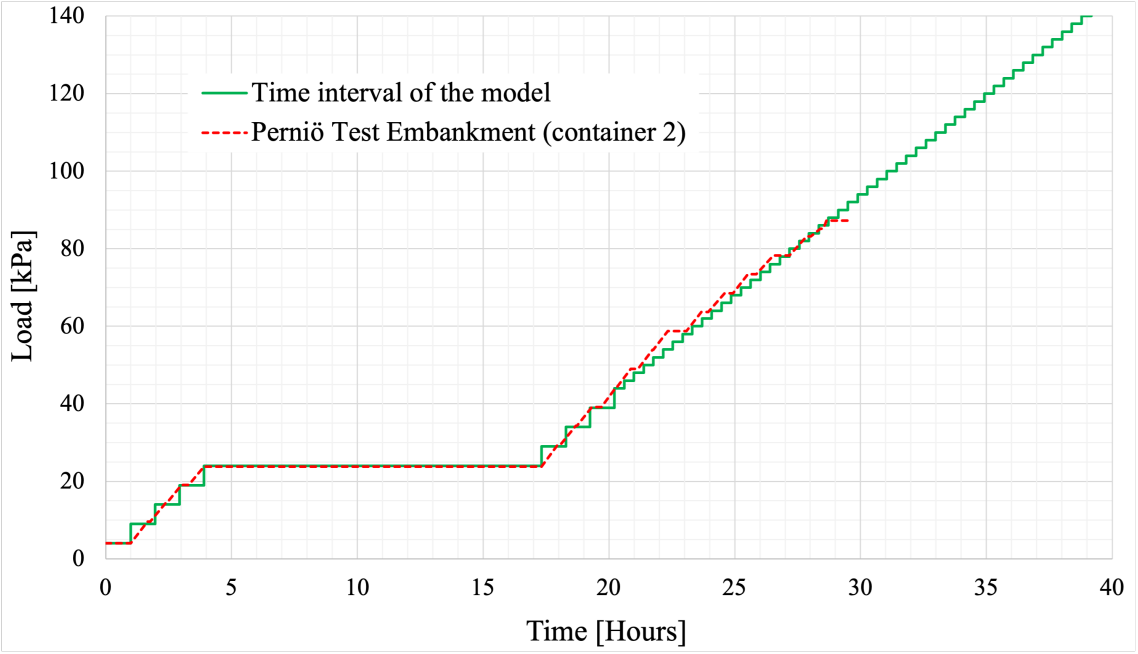

Figure 5.5: Graph of the load v.s. consolidation time interval of the model, compared to the Perniö test embankment.

For phase 1, the reset displacements to zero and reset small strain options were selected. This is since the purpose of the initial phase is not to calculate displacements, but rather the initial stresses.

For phase 2 and above, the pore pressure calculation type was set to phreatic. Furthermore, the updated mesh and updated water pressure options were selected. This is since the effect of the groundwater table following the displacements was required for the relatively large deformations expected. For more detailed information, see Table 5.7.

Table 5.7: Settings for phase 1 to 70.

	Phase 1	**Phase 2-70**
General		
Calculation type	Consolidation	
Loading type	Staged construction	
ΣM_{weight}	1.00	
Pre pressure calculation type	Phreatic	
Deformation control parameters		
Force fully drained behaviour	Yes	
Reset displacements to zero	Yes	No
Reset small strain	Yes	No
Reset state variables	No	
Reset time	No	
Updated mesh	Yes	
Updated water pressure	Yes	
Ignore suction	Yes	
Cavitation cut-off	No	
Numerical control parameters		
Max cores to use	256	
Max number of steps stored	1	
Use default iter parameters	Yes	

5.8 Model behaviour

The excess pore pressures at the phases before loading and before failure can be seen in Figures 5.6 and 5.7, respectively. For the phase before loading, the largest excess pore pressure is equal to -18.87 kN/m^2. From the Figure 5.6, it can be seen that the excess pore pressure is highest under the embankment and has a lower value under the excavation. The excess pore pressure increases with the load, and the highest value at the phase before failure is -68.78 kN/m^2. The excess pore pressures are equal to 0 kN/m^2 at the horizontal boundaries, X_{min} and X_{max}. This is due to the fact that the groundwater flow model conditions were set to open, which allows for flow and the excess pore water pressure to dissipate.

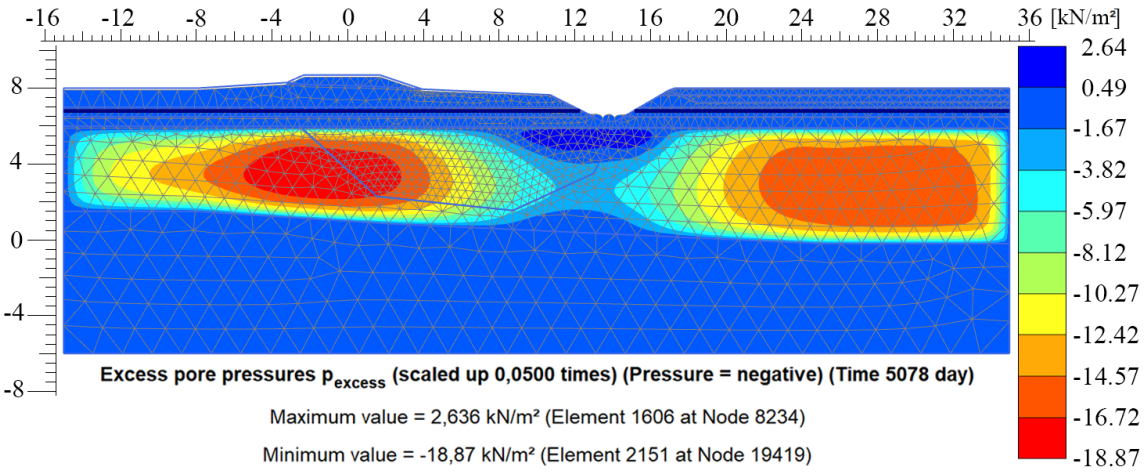

Figure 5.6: Excess pore pressure at the phase before loading.

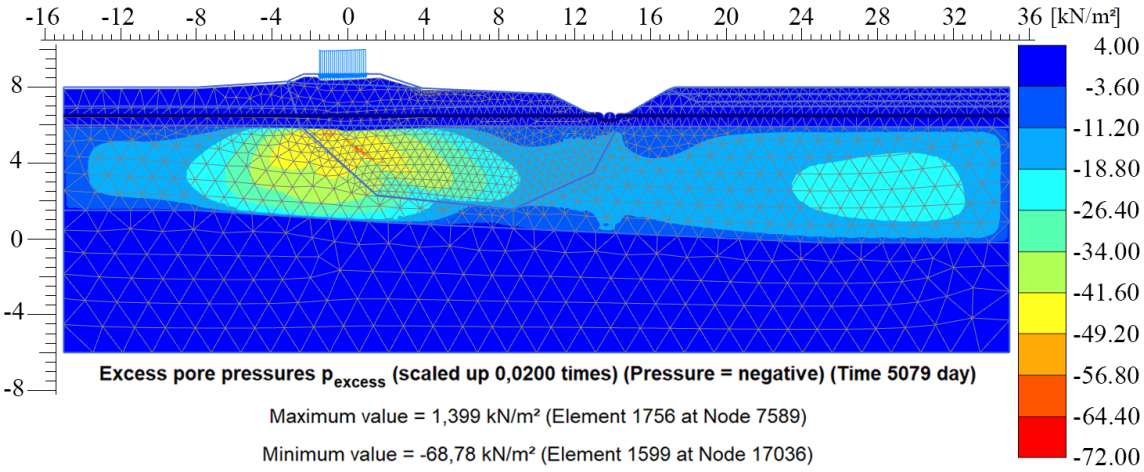

Figure 5.7: Excess pore pressure at the phase before failure.

The incremental displacements of the phase before and at failure can be seen in Figures 5.8 and 5.9, respectively. The slip surface is clear in both right before the failure, and at failure.

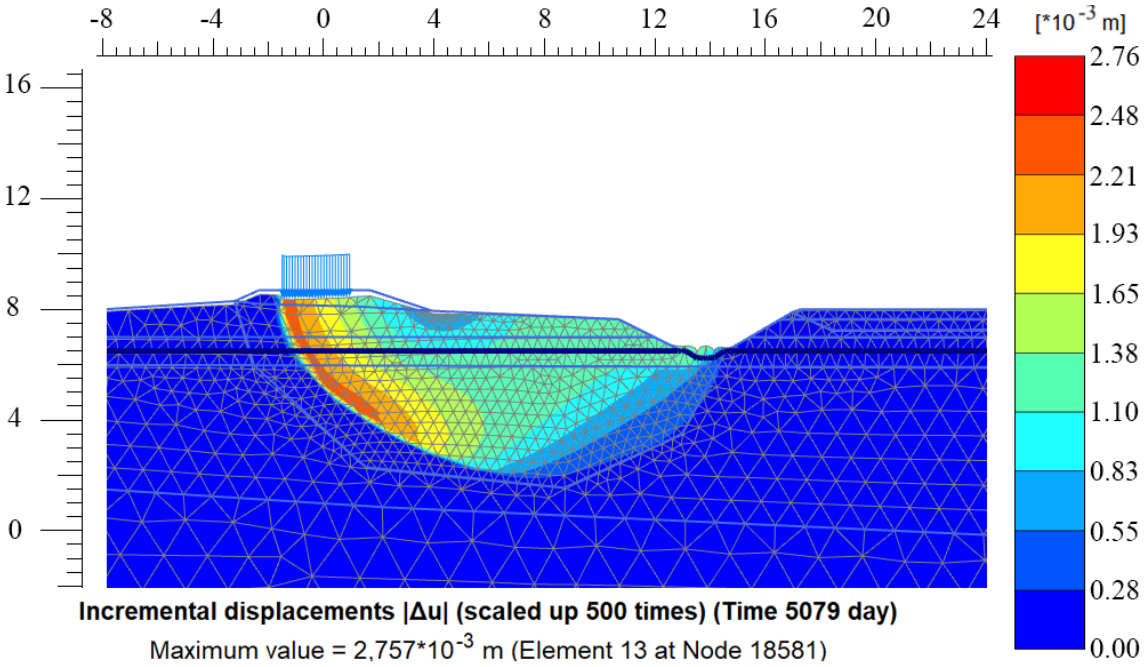

Figure 5.8: Incremental displacements at the phase before failure.

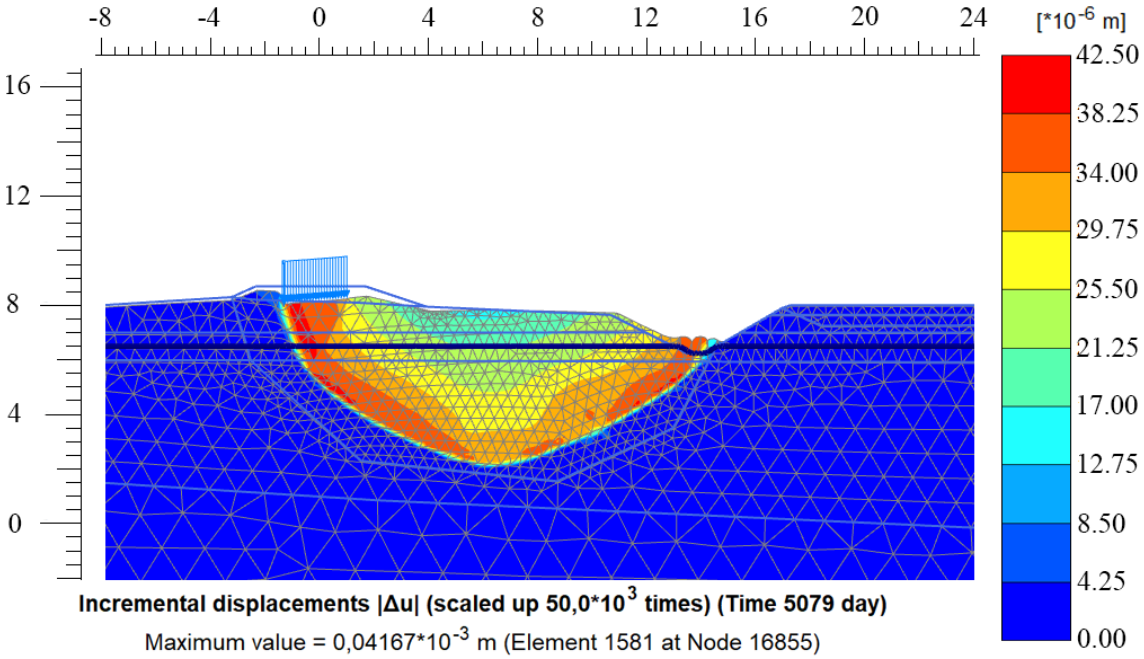

Figure 5.9: Incremental displacements at the failure phase.

A comparison between inclinometer data of the site and the PLAXIS 2D model was conducted. The placing of the inclinometers at the test site can be seen in Figure A.9, in the Appendix. In the PLAXIS 2D model, the horizontal locations of the inclinometers were at x = 4, 7.5 and 11 m, as shown in Figure 5.10. These locations corresponds to the test site (Lehtonen, 2011).

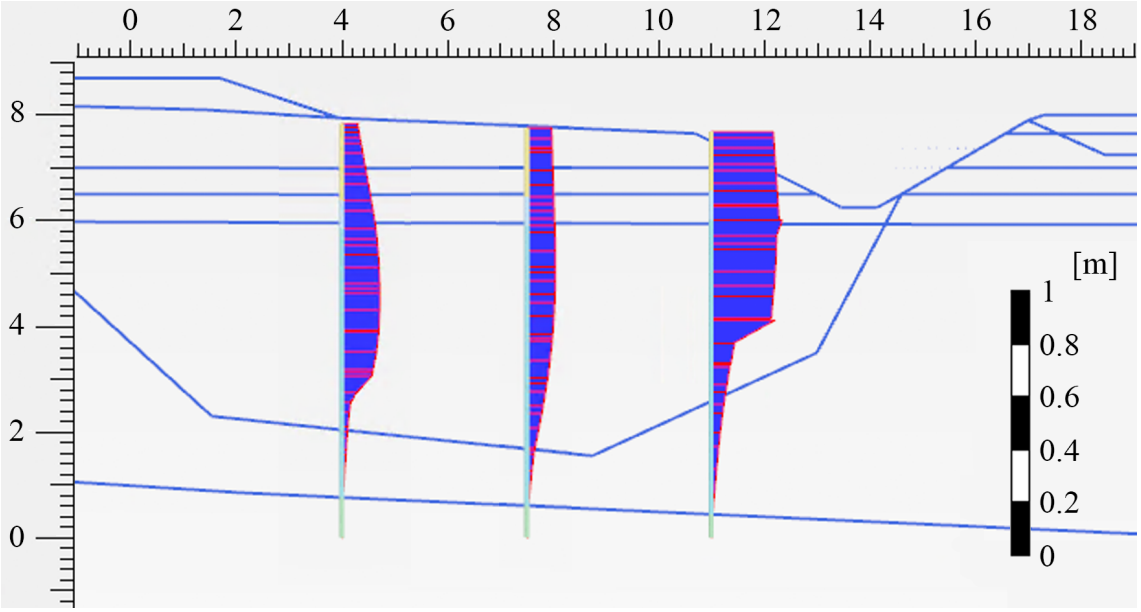

Figure 5.10: Inclinometer placement and horizontal displacements of the phase before failure.

The comparison between the inclinometer results and the PLAXIS 2D model showed similar behaviour for the horizontal displacements. However, the horizontal displacements were significantly larger for the model. See Figure 5.11.

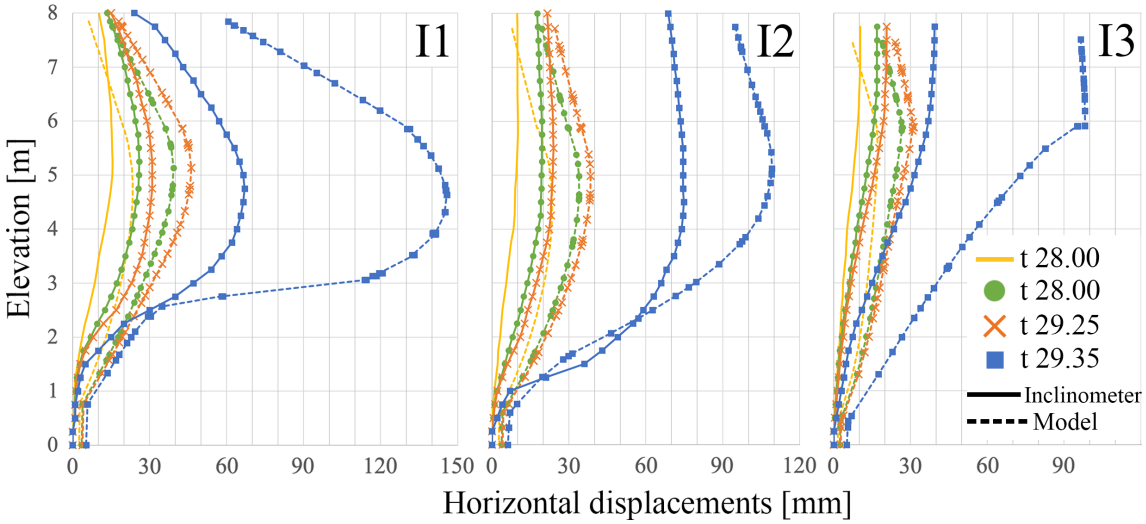

Figure 5.11: Horizontal displacement of the model compared to the inclinometer data of inclinometer 1, 2 and 3, respectively (Mataić et al., 2016).

A comparison between an oedometer test result and a simulation in SoilTest tool in PLAXIS was conducted. The oedometer test chosen was the oedometer test number 5861 from borehole 67-2010. It can be seen in Figure 5.1, marked in green with dotted lines and crosses. The sample was taken at a depth between 3.18 and 3.20 m.

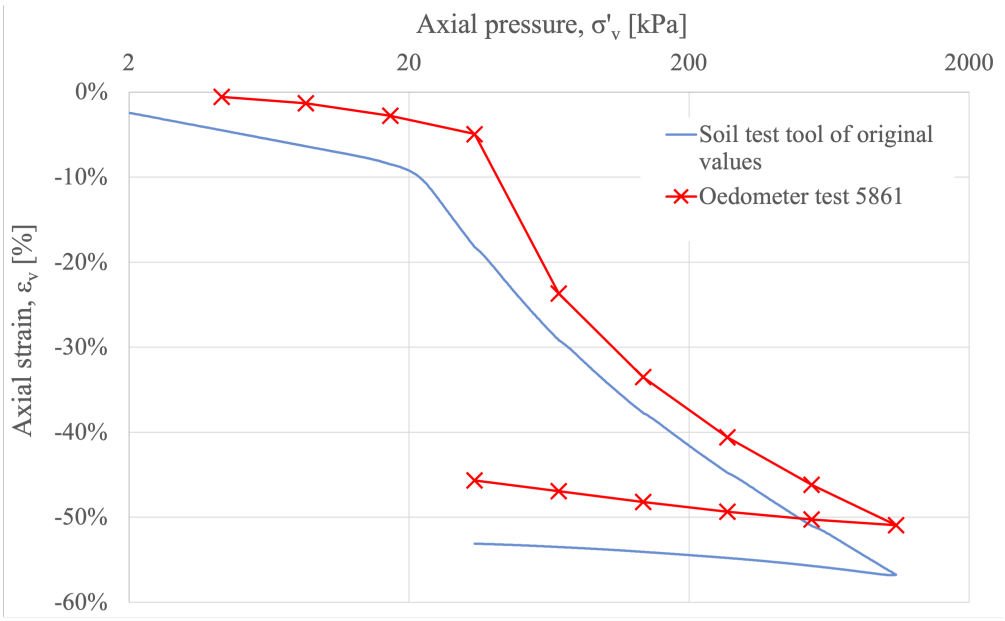

Figure 5.12: Comparison of an oedometer test result and a simulation in the SoilTest tool in PLAXIS.

To show how the material model behaves in an oedometer test when changing the parameters ±15 %, a SoilTest tool simulation in PLAXIS was conducted, varying POP, λ_i^* and κ^*. The results from the SoilTestTool can be seen in Figure 5.13.

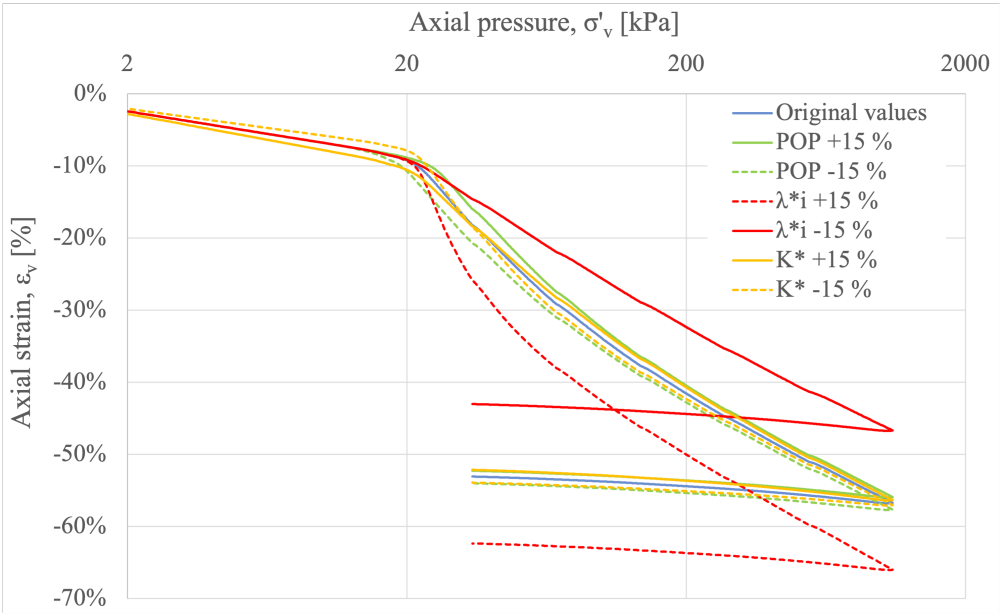

Figure 5.13: SoilTest tool.

The K_0-value, which generates the initial stresses, was calculated to 0.52 according to Equation 4.39, with an OCR of 1.45. A check was conducted to ensure that the vertical and the horizontal principal effective stresses are correctly calculated during the initial phase. The check shows that the initial phase has the expected K_0-value of 0.52. According to figures 5.14 and 5.15, the K_0-value is calculated to 0.52, and is hence reasonable.

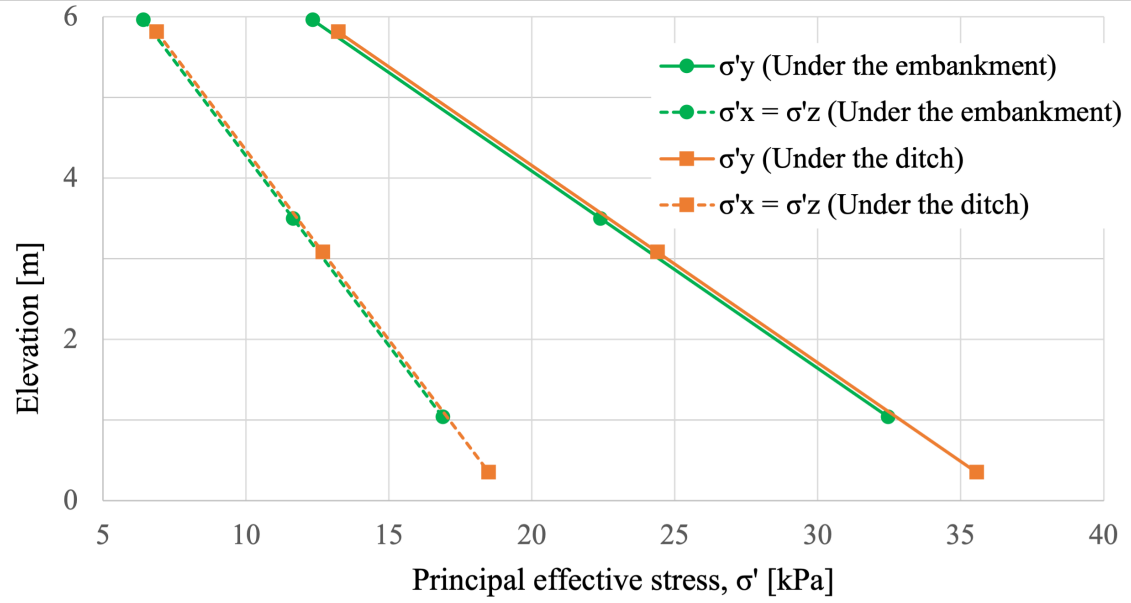

Figure 5.14: Principal stresses during the initial phase of the PLAXIS 2D model.

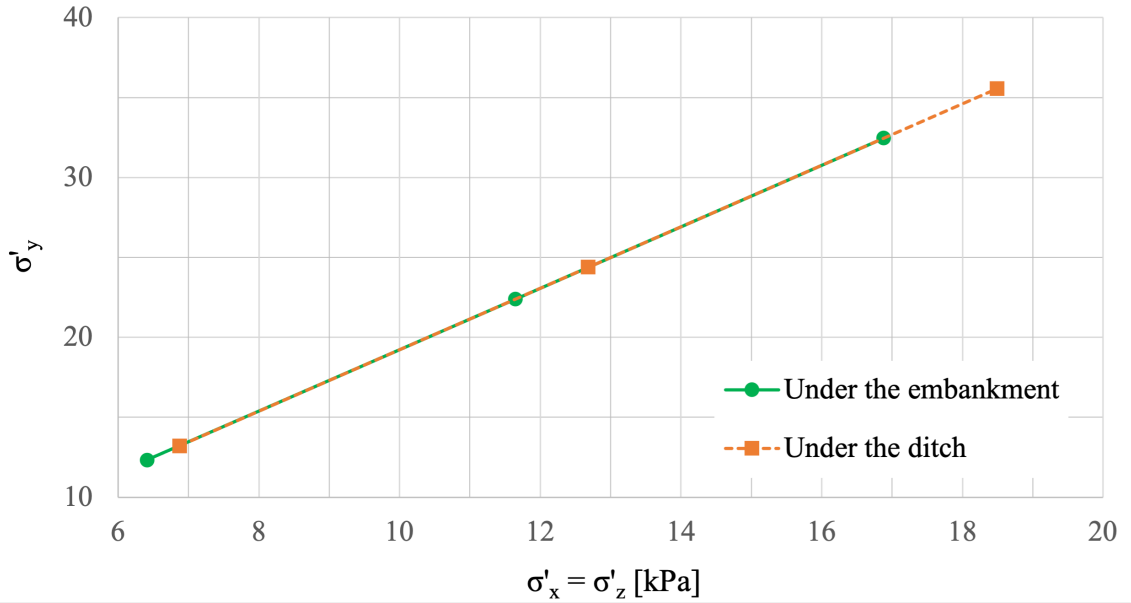

Figure 5.15: K_0 determination from the PLAXIS 2D model.

5.9 Design of Experiments

The sensitivity of the Creep-SCLAY1S model parameters were evaluated on a chosen response using factorial design. Initially fractional factorial design was utilized for all 13 model parameters in order to distinguish the important parameters. Afterwards, full factorial design was performed for the chosen important parameters to find out the most sensitive parameters regarding effect on the failure load.

5.9.1 Fractional factorial design

As an initial stage, 13 parameters were chosen to perform a two-level fractional factorial design. By using a fraction of full factorial design it is possible to estimate the main effects of each parameter only in 32 runs, instead of $2^{13} = 8192$ runs. A resolution of IV was utilized to do the fractional factorial design, where only the main effects of the parameters are used to do 2^{k-p} experiments. Therefore, the smallest number of runs are taken into account by choosing IV resolution. The interaction between main effects or between main effects and two-level interactions are not aliased with each other.

The selection of the basic design and independent generators need to be chosen for a 2^{k-p} experiment. Based on the theory behind the fractional factorial design, a $k = 13 - 8$ basic design and $p = 8$ independent generators need to plan for the sensitivity analysis. Table 5.8 shows the basic design and the subsequent generators for the the mentioned experiment.

Table 5.8: Fractional factorial design, 2^{13-8}_{IV} matrix.

Basic design					**Generators**							
a	b	c	d	e	f=abcde	g=abc	h=abd	i=abe	j=acd	k=ace	l=ade	m=bcd

Implementation of the design was done in Python using the PyDOE2 package (PyPI, 2021). Failure load representing the stability of the embankment was chosen as the response in order to evaluate the sensitivity of 13 model parameters. The fractional design is tabulated in Table 5.9, where "-" and "+" denote the lower and upper bounds, respectively.

Table 5.9: 2_{IV}^{13-8} Fractional factorial design matrix.

Run	κ^*	ν'	λ_i^*	M_c	M_e	ω	ω_d	ξ	ξ_d	POP	α_0	χ_0	μ_i^*
1	-	-	-	-	-	-	-	-	-	-	-	-	-
2	+	-	-	-	-	+	+	+	+	+	+	+	-
3	-	+	-	-	-	+	+	+	+	-	-	-	+
4	+	+	-	-	-	-	-	-	-	+	+	+	+
5	-	-	+	-	-	+	+	-	-	+	+	-	+
6	+	-	+	-	-	-	-	+	+	-	-	+	+
7	-	+	+	-	-	-	-	+	+	+	+	-	-
8	+	+	+	-	-	+	+	-	-	-	-	+	-
9	-	-	-	+	-	+	-	+	-	+	-	+	+
10	+	-	-	+	-	-	+	-	+	-	+	-	+
11	-	+	-	+	-	-	+	-	+	+	-	+	-
12	+	+	-	+	-	+	-	+	-	-	+	-	-
13	-	-	+	+	-	-	+	+	-	-	+	+	-
14	+	-	+	+	-	+	-	-	+	+	-	-	-
15	-	+	+	+	-	+	-	-	+	-	+	+	+
16	+	+	+	+	-	-	+	+	-	+	-	-	+
17	-	-	-	-	+	+	-	-	+	-	+	+	-
18	+	-	-	-	+	-	+	+	-	+	-	-	-
19	-	+	-	-	+	-	+	+	-	-	+	+	+
20	+	+	-	-	+	+	-	-	+	+	-	-	+
21	-	-	+	-	+	-	+	-	+	+	-	+	+
22	+	-	+	-	+	+	-	+	-	-	+	-	+
23	-	+	+	-	+	+	-	+	-	+	-	+	-
24	+	+	+	-	+	-	+	-	+	-	+	-	-
25	-	-	-	+	+	-	-	+	+	+	+	-	+
26	+	-	-	+	+	+	+	-	-	-	-	+	+
27	-	+	-	+	+	+	+	-	-	+	+	-	-
28	+	+	-	+	+	-	-	+	+	-	-	+	-
29	-	-	+	+	+	+	+	+	+	-	-	-	-
30	+	-	+	+	+	-	-	-	-	+	+	+	-
31	-	+	+	+	+	-	-	-	-	-	-	-	+
32	+	+	+	+	+	+	+	+	+	+	+	+	+

Four different analyses on all 13 Creep-SCLAY1S model parameters will be performed, named Analysis 1 to 4. The analyses will be performed by using fractional factorial design, with the design matrix as shown in Table 5.9. Different ranges of uncertainties were applied to the calibrated model parameters for Analysis 1 to 4. The calibrated model parameters, i.e. the reference set, is alternated to minimum and maximum levels. The range in terms of the bounds were chosen as 5.0, 7.5, 10.0, and 15.0 %, deviating from the originally derived values. The range of the bounds of Analysis 1 to 4 is shown in Table 5.10. A full list of the values for the model parameter ranges can be found in Appendix Table A.3.

Table 5.10: Upper and lower bounds of the model parameters used for Analysis 1 to 4.

	Defining of bounds
Analysis 1	±5.0 %
Analysis 2	±7.5 %
Analysis 3	±10.0 %
Analysis 4	±15.0 %

5.9.2 Full factorial design

Analyses with full factorial design was performed for the important parameters initiated from the fractional factorial design analyses. Same model responses were used to implement the full factorial design. The significant model parameters from the fractional design will be chosen for a full factorial design and their effects were altered alongside their interactions. Moreover, the consolidation time will be studied since there are uncertainties regarding the consolidation interval of the old fill layer. The old fill layer was added in Phase 1. More information regarding Phase 1 can be seen in Section 5.7.3. The parameters to be analysed can be seen in Table 5.11.

A full list of the values used as lower and upper bound for Analysis 5 and 6 can be seen in Table A.4, in the Appendix. For Analysis 5, the model parameters and the consolidation time are deviated in a range of ±10%. For Analysis 6, the four model parameters connected to the Creep-SCLAY1S were also deviated in the range of ±10%. However, a different approach for the variation of the consolidation time was utilized. This is due to the fact that a 10 % alteration of the consolidation time does only have a small impact as shown by the results of Analysis 5. Consolidation time have a quadratic relationship with dissipation of pore pressure (Verruijt, 2001). The quadratic behaviour of the consolidation time during small degrees of consolidation can be seen in Equation 5.1. In Equation 5.1, U stands for degree of consolidation, h for the thickness of the clay layer and c_v for the consolidation coefficient of the clay (Verruijt, 2001). Based on Equation 5.1, $(0.5\sqrt{t})^2$ and $(2\sqrt{t})^2$ were chosen as the lower and upper bounds for consolidation time respectively. However, altering the Creep-SCLAY1S model parameters in a 10 % percentile are shown to be reasonable according to the data of the site.

$$U = \frac{2}{\sqrt{\pi}}\sqrt{\frac{c_v t}{h^2}} \tag{5.1}$$

Table 5.11: Parameters set up for full factorial design for Analysis 5 and 6.

	Varied parameters
Analysis 5 and 6	λ_i^*, M_e, ξ, POP, consolidation time

For Analysis 5 and 6, based on the full factorial design theory with five parameters, a $2^5 = 32$ treatment combination are needed. The Python PyDOE2 package was used to implement the full factorial design. The full factorial design matrix can be seen in Table 5.12, where all main effects and their interactions are considered.

Table 5.12: 2^5 full factorial design.

Run	λ_i^*	M_e	ξ	POP	Time[1]
1	-	-	-	-	-
2	+	-	-	-	-
3	-	+	-	-	-
4	+	+	-	-	-
5	-	-	+	-	-
6	+	-	+	-	-
7	-	+	+	-	-
8	+	+	+	-	-
9	-	-	-	+	-
10	+	-	-	+	-
11	-	+	-	+	-
12	+	+	-	+	-
13	-	-	+	+	-
14	+	-	+	+	-
15	-	+	+	+	-
16	+	+	+	+	-
17	-	-	-	-	+
18	+	-	-	-	+
19	-	+	-	-	+
20	+	+	-	-	+
21	-	-	+	-	+
22	+	-	+	-	+
23	-	+	+	-	+
24	+	+	+	-	+
25	-	-	-	+	+
26	+	-	-	+	+
27	-	+	-	+	+
28	+	+	-	+	+
29	-	-	+	+	+
30	+	-	+	+	+
31	-	+	+	+	+
32	+	+	+	+	+

[1]Time refers to the time interval of the consolidation of phase 1. More info regarding phase 1 can be see as seen in Section 5.7.3.

5.10 PLAXIS 2D simulations

Automation was utilized for changing of the parameters due to the multiple number of parameters and their variations. Therefore, scripting were used to change the parameters, run the simulations, save the result, and repeat the process. In total, 192 PLAXIS 2D simulations were carried out for both the fractional and full factorial design to see the responses. Finally, to run the sensitivity analysis, failure phases for all runs were obtained and imported in PyDOE2 package alongside their design matrix.

6

Results & discussion

6.1 Fractional factorial design for analyses 1 to 4

6.1.1 Simulation responses

The responses, in terms of predicted failure load in each of the PLAXIS 2D simulation, or run, are shown in Figure 6.1. The response plotted on the vertical axis corresponds to the predicted failure load in kPa, for each run plotted on the horizontal axis. The details on the selected upper and lower bounds of the model parameters in each individual run is presented in the fractional factorial design Table 5.9. It can be seen in Figure 6.1 that there are clear trends and similar patterns in term of the failure load for the analyses. The change in the range of the responses are however noteworthy, not only the difference between the minimum and maximum predicted failure load increases when increasing the uncertainty bandwidth from ±5 to ±15 %, for the large uncertainty band in Analysis 4 also the mean is shifting downwards, i.e. on average the predicted failure load is lower than for the first 3 cases. The lowest failure load of 48 kPa is obtained for Analysis 4 when run number 7 and 13 is performed. The highest failure load of 120 kPa is obtained for Analysis 3, during the run number 27. A full table with the response of the experiments for Analysis 1 to 4 can be seen in the Appendix, Table A.1.

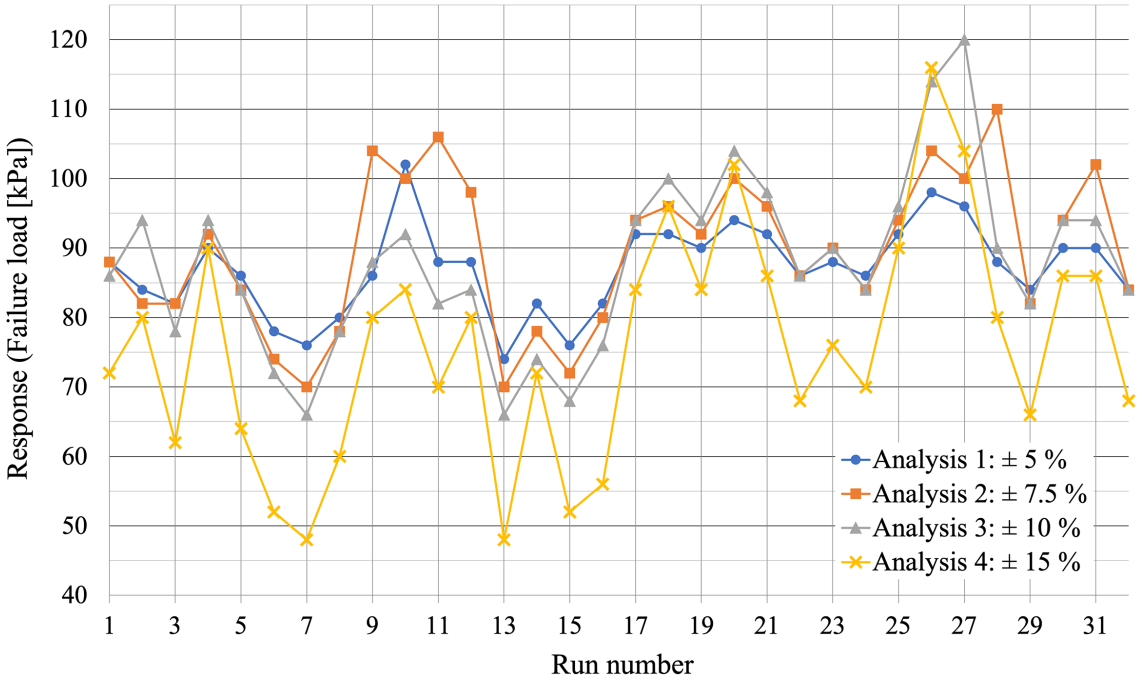

Figure 6.1: Response of the experiments for Analysis 1 to 4.

6.1.2 Effects of the parameters

The individual effects of the model parameters on the output are derived from the fractional factorial design method, using the PyDOE2 package in Python (PyPI, 2021). The effects of each parameter for Analyses 1 to 4 can be seen in Table 6.1. The effects correspond to the change in failure load when altering from the lower bound to the upper bound for each of the model parameters. Hence, a positive effect shows that an increase of the parameter value would result in a higher failure load. A negative value of the effect is the opposite and indicates that a higher value of the parameter would decrease the load required until failure is reached. Naturally, higher values of the effects would have higher influence on the response of the simulations. It's important to note that the effects presented are applicable for the geotechnical problem studied here, the stability of an embankment on soft soil.

Table 6.1: Effects of the parameters for Analysis 1 to 4 [kPa].

	Analysis 1	**Analysis 2**	**Analysis 3**	**Analysis 4**
κ^*	1.5	0.88	2.13	6.25
ν'_{ur}	-1.7	0.88	-2.13	-3.5
λ_i^*	-7.25	-13.63	-13.38	-20.5
M_c	1	5.63	0.13	2.75
M_e	6.25	9.38	15.13	19
ω	-0.75	-1.88	2.38	3
ω_d	1	-1.63	2.88	-0.25
ξ	-4.75	-4.88	-7.13	-11
ξ_d	-1.5	-3.13	-5.63	-6.25
POP	1.25	2.13	5.13	6.5
α_0	0	-4.63	-0.38	-2.75
χ_0	-1.75	1.13	-0.38	-0.5
μ_i^*	2	1.63	2.38	3.75

Figure 6.2 shows the bar chart of the parameter effects, corresponding to Table 6.1. When taking all four analyses in consideration, the important parameters which are affecting the failure load the most are λ_i^*, M_e, ξ and POP. Also, parameters such as κ^*, M_c, ξ_d, α_0, and μ_i^* can be considered as influential parameters. The parameters ν'_{ur}, ω, ω_d, and χ_0 do not show any appreciable effects on the estimation of the failure load. The important effects of the important parameters are further discussed below:

- The model parameter λ_i^* can be determined as a very important factor affecting the estimation of the failure load in a significant way. The negative value of the effects for λ_i^* corresponds to a reverse relation where an increase of the parameter would result in a lower failure load. λ_i^* has a reverse relation with stiffness, meaning that when λ_i^* increases, the stiffness of the soil decreases. A lower stiffness also causes a higher creep rate. This relation would decrease the load needed before failure occurs.

- According to the effect, M_e can be determined as another significantly influential parameter on the prediction of the failure load. The reason for this occurrence is that the strength in extension, represented by M_e in the model, governs the mobilised strength along large part of the failure plane, that for this case is shallow. The equation used to calculate M_e, in absence of laboratory data, i.e. Equation 4.31, will underestimate the value of M_e (Karstunen and Amavasai, 2017). Figure 6.2 shows that an increase of M_e has a large positive effect within this kind of geotechnical related problems. An overestimation might hence be unsafe and it would be reasonable to underestimate M_e.

- The parameters ξ and ξ_d are also shown to be important, however with less effect than λ_i^* and M_e. Note that ξ has a slightly more significant effect than ξ_d. ξ is calculated using the upper bound and lower bound values, as seen in Figure 5.2, and is also highly dependent on ξ_d. The upper bound and lower bound of ξ are 16.9 and 8.7, respectively. This accounts for a upper bound

that is almost double the lower bound. Therefore, the result is interesting due to the high uncertainties around determination of these parameters since they cannot be measured directly and optimisation needs to be carried out.

- POP does also have a dominant effect. This is interesting due to the fact that a deviation of ± 5 to 15 % is quite small compared to the scatter of the data acquired in Figure A.7. The scatter of POP for the samples are roughly 30 %, between the values 15 and 26 kPa. A higher POP would increase the overconsolidated region with swelling index (κ^*), where a higher stress would be needed before the compression index (λ^*) would begin. This can also be seen when varying POP in PLAXIS 2D SoilTest tool, Figure 5.13.

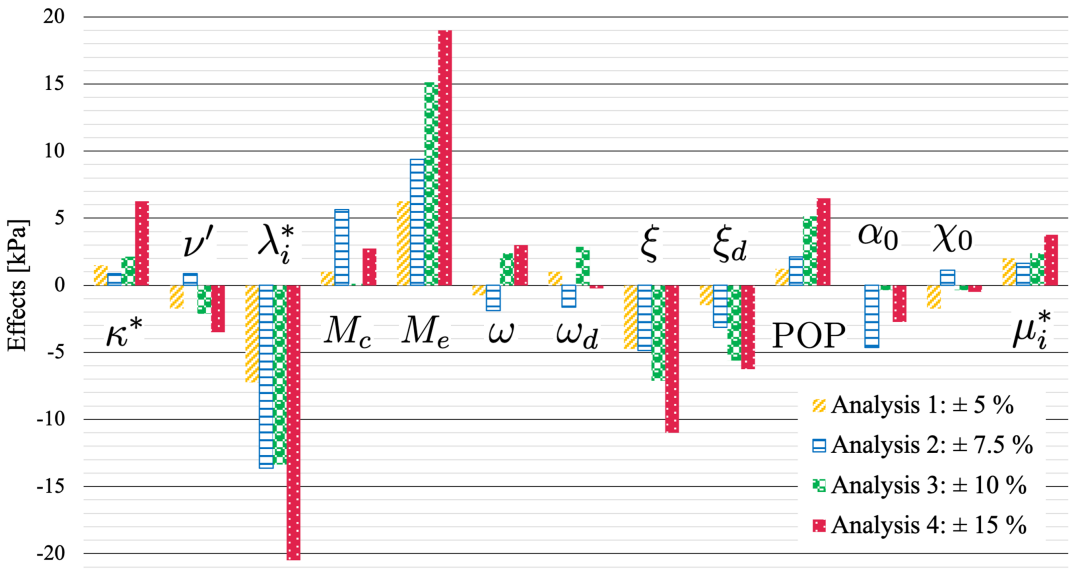

Figure 6.2: Effects of the parameters form fractional factorial design, Analysis 1 to 4.

6.2 Full factorial design for Analysis 5 & 6

6.2.1 Simulation responses

The responses of the PLAXIS 2D simulations for Analysis 5 and 6 are displayed in Figure 6.3. As in the previous fractional factorial design, the failure of the embankment during the loading stages are presented in the Figure. The patterns are similar for both analyses. However, for the simulations where the consolidation time was reduced, run 1 to 16, lower failure loads are obtained for Analysis 6 compared to Analysis 5. For the simulations where the consolidation time was increased, run 17 to 32, higher failure loads are reached. It is clear that the magnitude of the effective stress (or degree of consolidation) at the start of the failure test has a large impact on the results, especially when larger more realistic uncertainty bounds are taken into consideration.

The lowest responses have in common that M_e has a lower bound, and λ_i^* and ξ have upper bounds, i.e. low strength and low stiffness. Not surprisingly, the opposite is found for the highest responses where M_e has an upper bound, and λ_i^* and ξ have lower bounds. A full Table with the response of the experiments for Analysis 5 and 6 can be seen in the Appendix, Figure A.2.

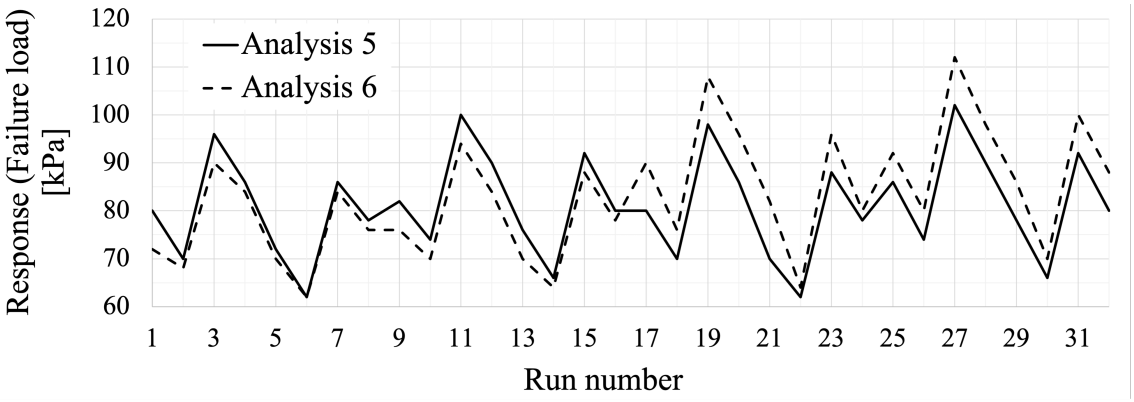

Figure 6.3: Response of the experiment for Analysis 5 and 6.

6.2.2 Effects of the parameters

The outcome of the full factorial design for the four Creep-SCLAY1S model parameters and the consolidation time is plotted in Figure 6.4. According to the effects for Analysis 5, M_e, λ_i^*, and ξ are the most important parameters with effects of 15.9, -10.4 and -8.3 kPa respectively. On the other hand, POP with a value of 4.1 kPa can still be considered an influential parameter on the estimation of the failure load.

The effects for Analysis 6 illustrate that M_e, the consolidation time, λ_i^*, and ξ are the most sensitive parameters with effects of 16.5, 11.75, -10.75 and -8.25 kPa, respectively. Also, POP can be considered a somewhat less influential parameter compared to the others. Detailed differences of the parameters are discussed below:

- For Analysis 5 and 6, where the full factorial design was implemented, M_e has the largest effect and λ_i^* is shown to be the second most important of the model parameters. This results differs from the fractional factorial design, where λ_i^* has the largest effect and M_e the second largest. A reason for this can be due to the effects of the full factorial design since all interactions and combinations of M_e are included in this kind of experiment. While fractional factorial design neglected some high-level interactions.

- ξ is the third most influential model parameter and has a negative effect on the responses of the failure load.

- When varying the consolidation time in a lower range, of $\pm$ 10 % as done in Analysis 5, the consolidation time for the old fill is not as important, compared to the four model parameters. However, the consolidation time is shown to be

a important factor when varied as according to Analysis 6, where a substantial effect of consolidation is designed in the full factorial experiment.

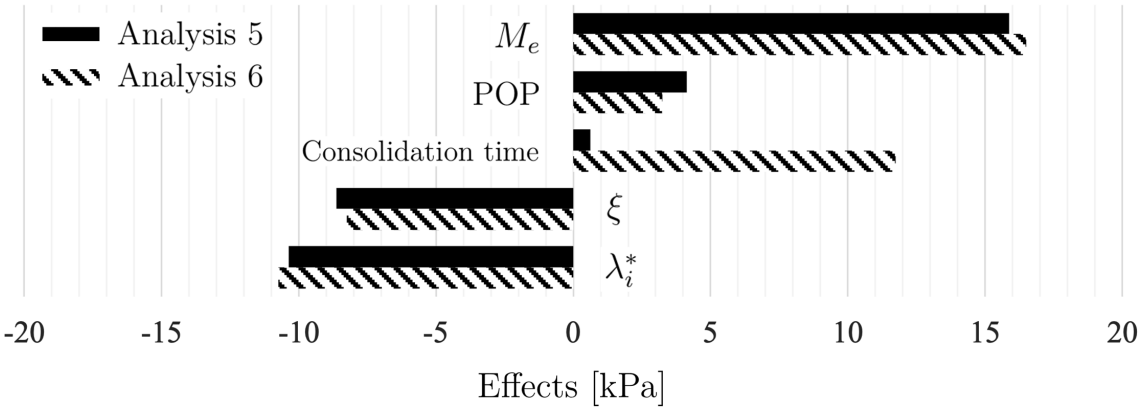

Figure 6.4: Effects of the parameters from full factorial design, Analysis 5 and 6.

7
Conclusions

In this work a Global Sensitivy Analysis on the numerical simulation of the failure test on the Perniö test embankment was performed. The focus was on quantifying the sensitivity of the model parameters of Creep-SCLAY1s on the predicted failure load. The PLAXIS 2D Finite Element code was used for all analyses.

The required model parameters and soil properties were first interpreted with the help of available data. The model was calibrated numerically against experimental data using the PLAXIS 2D SoilTest tool. Subsequently, the numerical model was further calibrated at boundary value level using the available data from the field test and prior research findings.

The quantification of the importance of the model parameters in the Creep-SCLAY1S model on the predicted failure load was done using fractional factorial design, where λ_i^*, M_e, ξ and POP were identified as the most significant factors. Once the important parameters are highlighted, another more detailed global sensitivity analysis was carried out for the selected parameters, using full factorial design. In this analysis the impact of the consolidation time of the old fill prior to the embankment test was also investigated. For both fractional and full factorial design, the sensitivity results show similar trends for the importance of parameters. From the current analyses it becomes apparent that the slope stability of embankments on soft soils is dependent on behaviour connected to strength, destructuration and compressibility of the clay layer. Parameters governing the anisotropy and stiffness in the overconsolidated range have less effects on the stability. Regarding the consolidation time of the old fill, there is a clear effect when using the more realistic ranges, as evaluated in Analysis 6. However, smaller variations regarding the consolidation time are shown to have substantially less effect on this type of geotechnical related analysis.

Most importantly, the results presented herein demonstrate that the strength in extension, controlled by M_e in the model, has a large effect onf the stability of the test embankment studied. Therefore, for these type of problems it would be essential to specify anisotropically consolidated undrained triaxial tests loaded in extension. Although this is commonly done in Sweden, this was not the case for Finland for which at the time of writing only limited data was available and triaxial extension tests are not performed routinely.

Another important outcome is that the full factorial design shows more accurate results, compared to fractional factorial design, where all parameter interactions

and their interactions are considered in the analysis. However, the large number of simulations required for this kind of analysis makes this approach computationally expensive. It, therefore, is recommended to perform a full factorial design after screening the non-important parameters using fractional factorial design. A full factorial design on all Creep-SCLAY1S model parameters should be performed to confirm that this two step approach (as followed in this research) indeed yields a similar outcome.

Other methods to conduct global sensitivity analyses could be used to verify the results presented. Regardliess this study shows that caution should be taken regarding evaluation of model parameters, when building embankments on soft soil. Overestimation or underestimation of the parameters can easily lead to unsafe conditions. It therefore is recommended to include uncertainties in a quantifiable manner when performing geotechnical analysis.

Bibliography

Box, G. E., & Hunter, J. S. (1961). The 2 k—p fractional factorial designs. *Taylor & Francis Group*, *3*(3), 311–351.

Carlsten, P., & Henriksson, T. (1994). Lagringstidens inverkan på prover tagna med standardkolvprovtagare (in swedish). english title: The effect of storage time of samples taken with the standard piston sampler. *Swedish Geotechnical Institute*.

Christopher Frey, H., & Patil, S. R. (2002). Identification and review of sensitivity analysis methods. *Wiley Online Library*, *22*(3), 553–578.

Cox, D. R. (1958). Planning of experiments. *Wiley*.

Craig, R. F., & Knappett, J. (2012). *Craig's soil mechanics* (Vol. 8). Spon press.

Cullen, A. C., Frey, H. C., & Frey, C. H. (1999). *Probabilistic techniques in exposure assessment: A handbook for dealing with variability and uncertainty in models and inputs*. Springer Science & Business Media.

Dijkstra, J. (2019a). Ace045 geotech si. *Course ACE045 Geological and geotechnical site characterisation, Chalmers University of Technology, Gothenburg*.

Dijkstra, J. (2019b). Ace045 revision. *Course ACE045 Geological and geotechnical site characterisation, Chalmers University of Technology, Gothenburg*.

Douglas, C. M. (2013). *Design and analysis of experiments*. John Wiley; Sons & Singapore Pte.Ltd.

Eckhardt, J., & Rantala, J. (2012). The role of intelligent logistics centres in a multimodal and cost-effective transport system. *Elsevier*, *48*, 612–621.

ETSC. (2003). Transport safety performance in the eu - a statistical overview. *European Transport Safety Council, Brussels*.

Fetter, C. W. (2018). *Applied hydrogeology*. Waveland Press.

Gras, J.-P., Sivasithamparam, N., Karstunen, M., & Dijkstra, J. (2017). Strategy for consistent model parameter calibration for soft soils using multi-objective optimisation. *Elsevier*, *90*, 164–175.

Gras, J.-P., Sivasithamparam, N., Karstunen, M., & Dijkstra, J. (2018). Permissible range of model parameters for natural fine-grained materials. *Springer*, *13*(2), 387–398.

Gunst, R. F., & Mason, R. L. (2009). Fractional factorial design. *Wiley Online Library*, *1*(2), 234–244.

Hamby, D. M. (1994). A review of techniques for parameter sensitivity analysis of environmental models. *Springer*, *32*(2), 135–154.

Hoffman, F., & Gardner, R. (1983). Evaluation of uncertainties in environmental radiological assessment models. *US Nuclear Regulatory Commission Washington, DC*, *11*, 1.

Iman, R. L., & Helton, J. C. (1988). An investigation of uncertainty and sensitivity analysis techniques for computer models. *Wiley Online Library*, *8*(1), 71–90.

Karlsson, M., & Moritz, L. (2016). Trafikverkets tekniska krav för geokonstruktioner, tk geo 13. *Trafikverket, tekn. rapport*, (TDOK 2013:0667 Version 2.0).

Karstunen, M., & Amavasai, A. (2017). Best soil: Soft soil modelling and parameter determination.

Laera, A., Sarathchandran, A., & Brinkgreve, R. (2018). Plaxis the creep-sclay1s model 2018. *Plaxis bv*.

Lehtonen, V. (2011). Instrumentation and analysis of a railway embankment failure experiment: A general summary. *Liikenneviraston tutkimuksia ja selvityksiä: 29/2011*.

Lehtonen, V., Meehan, C., Länsivaara, T., & Mansikkamäki, J. (2015). Full-scale embankment failure test under simulated train loading. *Thomas Telford Ltd*, *65*(12), 961–974.

Leoni, M., Karstunen, M., & Vermeer, P. (2008). Anisotropic creep model for soft soils. *Thomas Telford Ltd*, *58*(3), 215–226.

Lunne, T., Berre, T., & Strandvik, S. (1997). Sample disturbance effects in soft low plastic norwegian clay.

Mansikkamäki, J. (2015). Effective stress finite element stability analysis of an old railway embankment on soft clay. *Tampere University of Technology*.

Mataić, I. et al. (2016). On structure and rate dependence of perniö clay. *Aalto University*.

Mee, R. (2009). *A comprehensive guide to factorial two-level experimentation*. Springer Science & Business Media.

Plaxis. (2019a). Plaxis 2d reference manual 2019. *Plaxis bv*.

Plaxis. (2019b). Plaxis material models manual 2019. *Plaxis bv*.

PyPI. (2021). *Pydoe2: An experimental design package for python* (The Python Package Index, Ed.) [Accessed: 2021-03-10]. https://pypi.org/project/pyDOE2/

Saltelli, A. (2004). Global sensitivity analysis: An introduction. *Proc. 4th International Conference on Sensitivity Analysis of Model Output (SAMO'04)*, *27*, 43.

Saltelli, A., Tarantola, S., Campolongo, F., & Ratto, M. (2004). *Sensitivity analysis in practice: A guide to assessing scientific models* (Vol. 1). Wiley Online Library.

Sivasithamparam, N., Karstunen, M., & Bonnier, P. (2015). Modelling creep behaviour of anisotropic soft soils. *Elsevier*, *69*, 46–57.

Sudret, B. (2008). Global sensitivity analysis using polynomial chaos expansions. *Reliability engineering & system safety*, *93*(7), 964–979.

Tian, W. (2013). A review of sensitivity analysis methods in building energy analysis. *Renewable and Sustainable Energy Reviews*, *20*, 411–419.

Tjie-Liong, G. (2014). Common mistakes on the application of plaxis 2d in analyzing excavation problems. *International Journal of Applied Engineering Research*, *9*(21), 8291–8311.

van der Sloot, M. (2020). *Udsm - creep-sclay1s* (Bentley Communities, Ed.) [Accessed: 2021-03-15]. https://communities.bentley.com/products/geotech-analysis/w/plaxis-soilvision-wiki/46106/udsm---creep-sclay1s

Verruijt, A. (2001). *Soil mechanics*. Delft University of Technology Delft.

Vozniak, E., Burgundosova, A., & Kopytova, A. (2018). Adaptation and reconstruction of the stations on the finland railway road. *MATEC Web of Conferences*, *239*, 01016.

Wheeler, S. J., Näätänen, A., Karstunen, M., & Lojander, M. (2003). An anisotropic elastoplastic model for soft clays. *NRC Research Press Ottawa, Canada*, *40*(2), 403–418.

Zangeneh, N., Azizian, A., Lye, L., Popescu, R., et al. (2002). Application of response surface methodology in numerical geotechnical analysis. *Proc. 55th Canadian Society for Geotechnical Conference, Hamilton*.

A

Appendix 1

A.1 Response of the experiments

Table A.1: Response of the experiments for Analysis 1 to 4.

														Response in kPa, Analysis number:			
Run	κ^*	ν'	λ_i^*	M_c	M_e	ω	ω_d	ξ	ξ_d	POP	α_0	χ_0	μ_i^*	**1**	**2**	**3**	**4**
1	-	-	-	-	-	-	-	-	-	-	-	-	-	88	88	86	72
2	+	-	-	-	-	+	+	+	+	+	+	+	-	84	82	94	80
3	-	+	-	-	-	+	+	+	+	-	-	-	+	82	82	78	62
4	+	+	-	-	-	-	-	-	-	+	+	+	+	90	92	94	90
5	-	-	+	-	-	+	+	-	-	+	+	-	+	86	84	84	64
6	+	-	+	-	-	-	-	+	+	-	-	+	+	78	74	72	52
7	-	+	+	-	-	-	-	+	+	+	+	-	-	76	70	66	48
8	+	+	+	-	-	+	+	-	-	-	-	+	-	80	78	78	60
9	-	-	-	+	-	+	-	+	-	+	-	+	+	86	104	88	80
10	+	-	-	+	-	-	+	-	+	-	+	-	+	102	100	92	84
11	-	+	-	+	-	-	+	-	+	+	-	+	-	88	106	82	70
12	+	+	-	+	-	+	-	+	-	-	+	-	-	88	98	84	80
13	-	-	+	+	-	-	+	+	-	-	+	+	-	74	70	66	48
14	+	-	+	+	-	+	-	-	+	+	-	-	-	82	78	74	72
15	-	+	+	+	-	+	-	-	+	-	+	+	+	76	72	68	52
16	+	+	+	+	-	-	+	+	-	+	-	-	+	82	80	76	56
17	-	-	-	-	+	+	-	-	+	-	+	+	-	92	94	94	84
18	+	-	-	-	+	-	+	+	-	+	-	-	-	92	96	100	96
19	-	+	-	-	+	-	+	+	-	-	+	+	+	90	92	94	84
20	+	+	-	-	+	+	-	-	+	+	-	-	+	94	100	104	102
21	-	-	+	-	+	-	+	-	+	+	-	+	+	92	96	98	86
22	+	-	+	-	+	+	-	+	-	-	+	-	+	86	86	86	68
23	-	+	+	-	+	+	-	+	-	+	-	+	-	88	90	90	76
24	+	+	+	-	+	-	+	-	+	-	+	-	-	86	84	84	70
25	-	-	-	+	+	-	-	+	+	+	+	-	+	92	94	96	90
26	+	-	-	+	+	+	+	-	-	-	-	+	+	98	104	114	116
27	-	+	-	+	+	+	+	-	-	+	+	-	-	96	100	120	104
28	+	+	-	+	+	-	-	+	+	-	-	+	-	88	110	90	80
29	-	-	+	+	+	+	+	+	+	-	-	-	-	84	82	82	66
30	+	-	+	+	+	-	-	-	-	+	+	+	-	90	94	94	86
31	-	+	+	+	+	-	-	-	-	-	-	-	+	90	102	94	86
32	+	+	+	+	+	+	+	+	+	+	+	+	+	84	84	84	68

Table A.2: Response of the experiments for Analysis 5 and 6.

						Response of		
Run	λ_i^*	M_e	ξ	POP	Time[1]	**Analysis 5**	**Analysis 6**	
1	-	-	-	-	-	80	72	kPa
2	+	-	-	-	-	70	68	kPa
3	-	+	-	-	-	96	90	kPa
4	+	+	-	-	-	86	84	kPa
5	-	-	+	-	-	72	70	kPa
6	+	-	+	-	-	62	62	kPa
7	-	+	+	-	-	86	84	kPa
8	+	+	+	-	-	78	76	kPa
9	-	-	-	+	-	82	76	kPa
10	+	-	-	+	-	74	70	kPa
11	-	+	-	+	-	100	94	kPa
12	+	+	-	+	-	90	84	kPa
13	-	-	+	+	-	76	70	kPa
14	+	-	+	+	-	66	64	kPa
15	-	+	+	+	-	92	88	kPa
16	+	+	+	+	-	80	78	kPa
17	-	-	-	-	+	80	90	kPa
18	+	-	-	-	+	70	76	kPa
19	-	+	-	-	+	98	108	kPa
20	+	+	-	-	+	86	96	kPa
21	-	-	+	-	+	70	82	kPa
22	+	-	+	-	+	62	64	kPa
23	-	+	+	-	+	88	96	kPa
24	+	+	+	-	+	78	80	kPa
25	-	-	-	+	+	86	92	kPa
26	+	-	-	+	+	74	80	kPa
27	-	+	-	+	+	102	112	kPa
28	+	+	-	+	+	90	98	kPa
29	-	-	+	+	+	78	86	kPa
30	+	-	+	+	+	66	70	kPa
31	-	+	+	+	+	92	100	kPa
32	+	+	+	+	+	80	88	kPa

[1]Time refers to the time interval of the consolidation of phase 1. More info regarding phase 1 can be see as seen in Section 5.7.3.

A.2 Lower and upper bounds used for the analyses

Table A.3: Lower and upper bound values used for Analysis 1 to 4. The variation of the lower and upper bound values are ±5.0, ±7.5, ±10.0, and ±15.0 % from the originally derived values, for Analysis 1, 2, 3 and 4, respectively. The unit of POP is kPa, the rest of the model parameters are unitless.

		Analysis 1		**Analysis 2**		**Analysis 3**		**Analysis 4**	
	Original value	**Lower bound**	**Upper bound**	**Lower bound**	**Upper bound**	**Lower bound**	**Upper bound**	**Lower bound**	**Upper bound**
κ^*	0.027	0.02565	0.02835	0.02498	0.02903	0.0243	0.0297	0.02295	0.03105
ν'_{ur}	0.15	0.1425	0.1575	0.13875	0.16125	0.135	0.165	0.1275	0.1725
λ_i^*	0.076	0.0722	0.0798	0.0703	0.0817	0.0684	0.0836	0.0646	0.0874
M_c	1.40	1.33	1.47	1.295	1.505	1.26	1.54	1.19	1.61
M_e	0.95	0.9025	0.9975	0.87875	1.02125	0.855	1.045	0.8075	1.0925
ω	51.93	49.305	54.495	48.0075	55.7925	46.71	57.09	44.115	59.685
ω_d	0.94	0.9025	0.9975	0.87875	1.02125	0.855	1.045	0.8075	1.0925
ξ	12.8	12.160	13.440	11.84	13.76	11.52	14.08	10.880	14.720
ξ_d	0.2	0.19	0.21	0.185	0.215	0.18	0.22	0.17	0.23
POP	19.0	18.05	19.95	17.575	20.425	17.1	20.9	16.15	21.85
α_0	0.54	0.513	0.567	0.4995	0.5805	0.486	0.594	0.459	0.621
χ_0	38	36.1	39.9	35.15	40.85	34.2	41.8	32.3	43.7
μ_i^*	0.0026	0.00247	0.00273	0.002405	0.002795	0.00234	0.00286	0.00221	0.00299

Table A.4: Lower and upper bound values used for Analysis 5 and 6.

		Analysis 5		**Analysis 6**		
	Original value	**Lower bound**	**Upper bound**	**Lower bound**	**Upper bound**	***Unit***
λ_i^*	0.076	0.0684	0.0836	0.0684	0.0836	–
M_e	0.95	0.855	1.045	0.855	1.045	–
ξ	12.8	11.52	14.08	11.52	14.08	–
POP	19	17.1	20.9	17.1	20.9	*kPa*
Consolidation time	5000	4500	5500	1225	19600	*Days*

A.3 Samples and laboratory test results

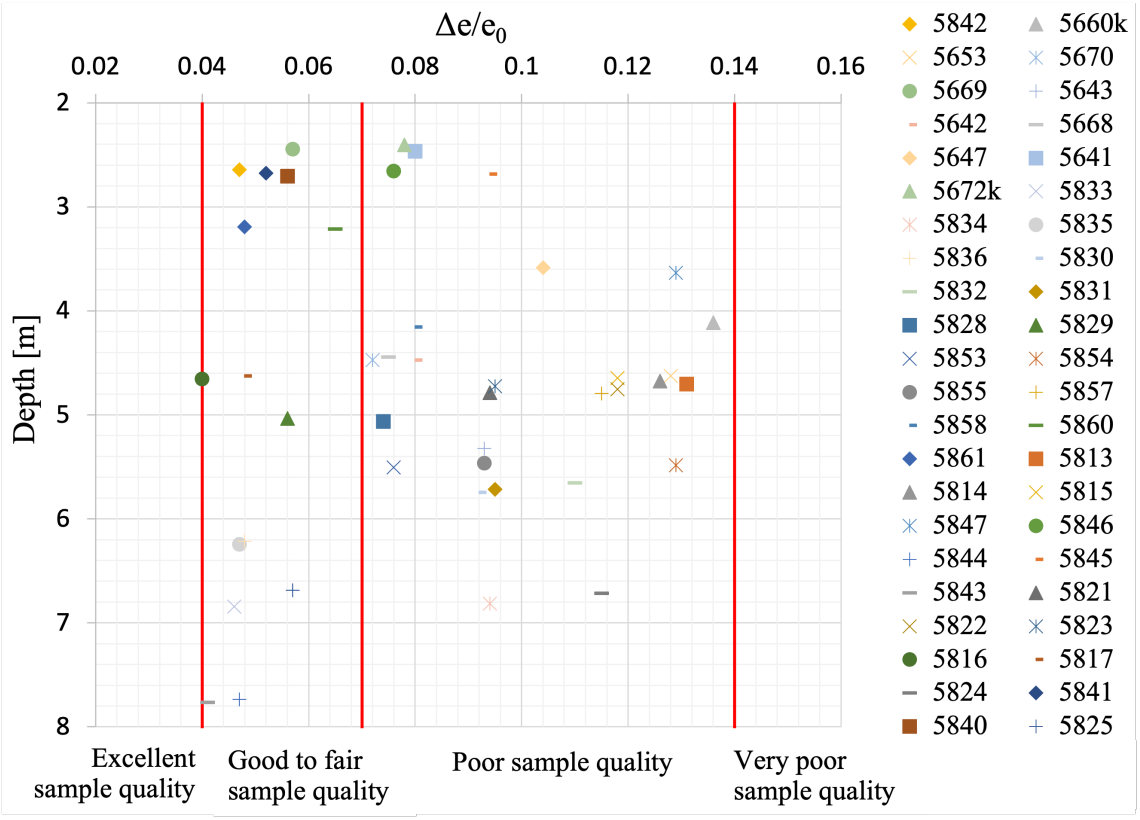

Figure A.1: Sample quality test of the Incremental loading oedometer tests, according to the $\Delta e/e_0$ criterion.

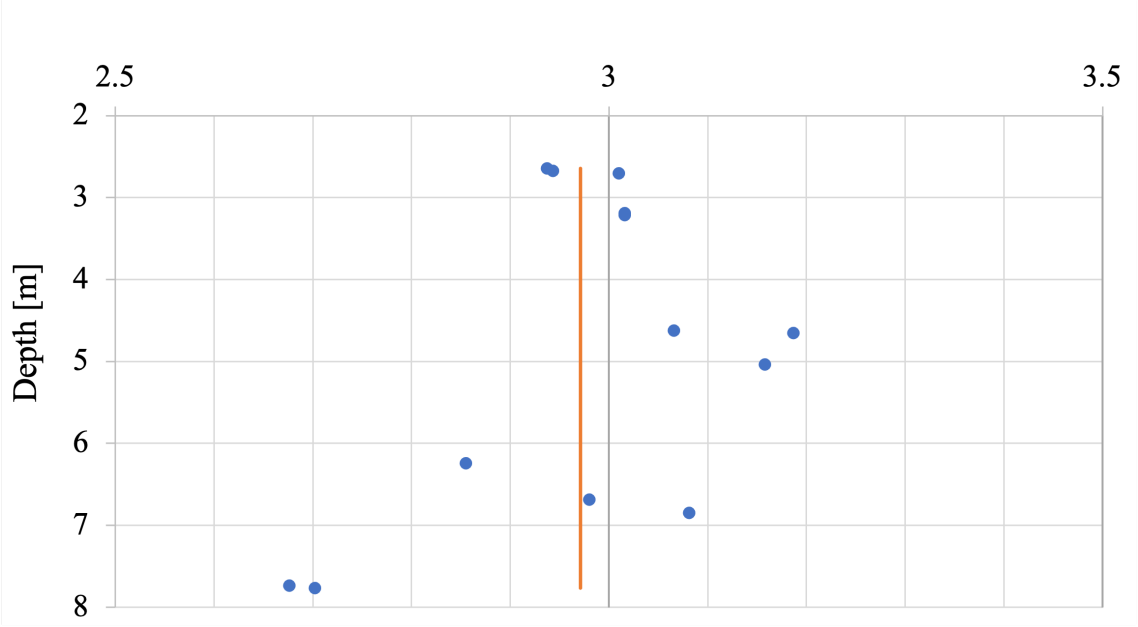

Figure A.2: Initial void ratio of samples with good to fair quality.

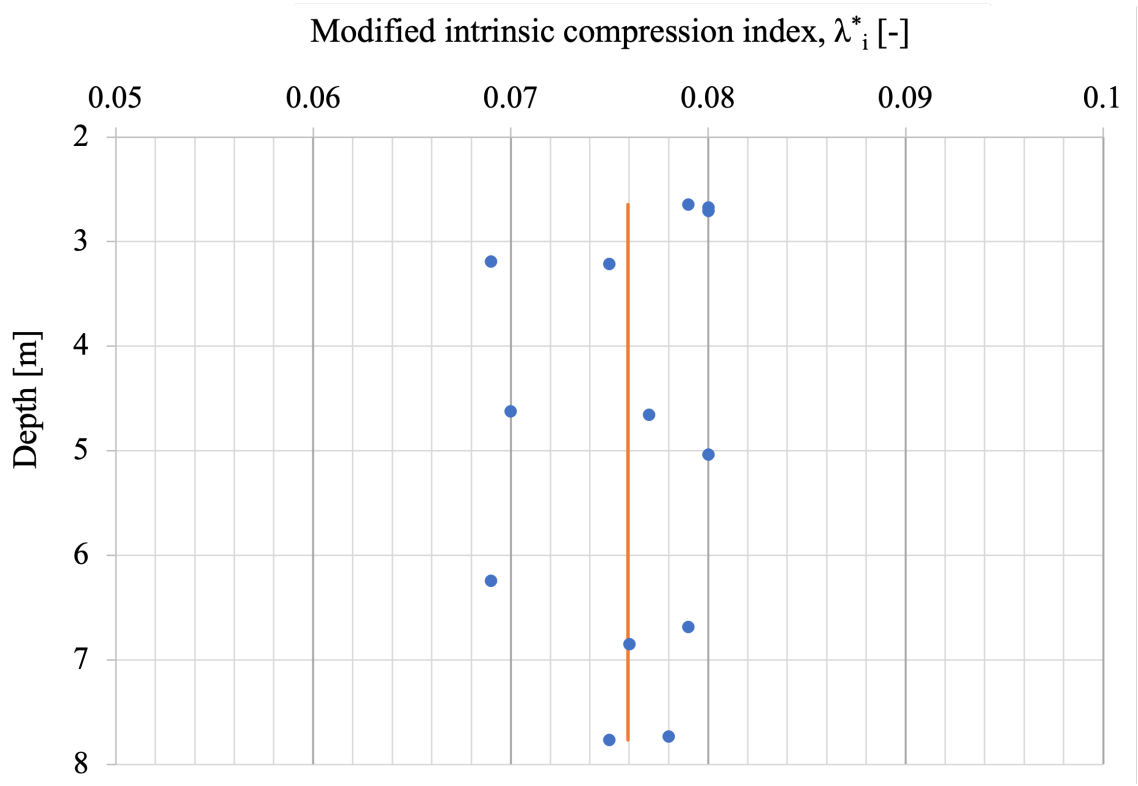

Figure A.3: λ_i^* of samples with good to fair quality.

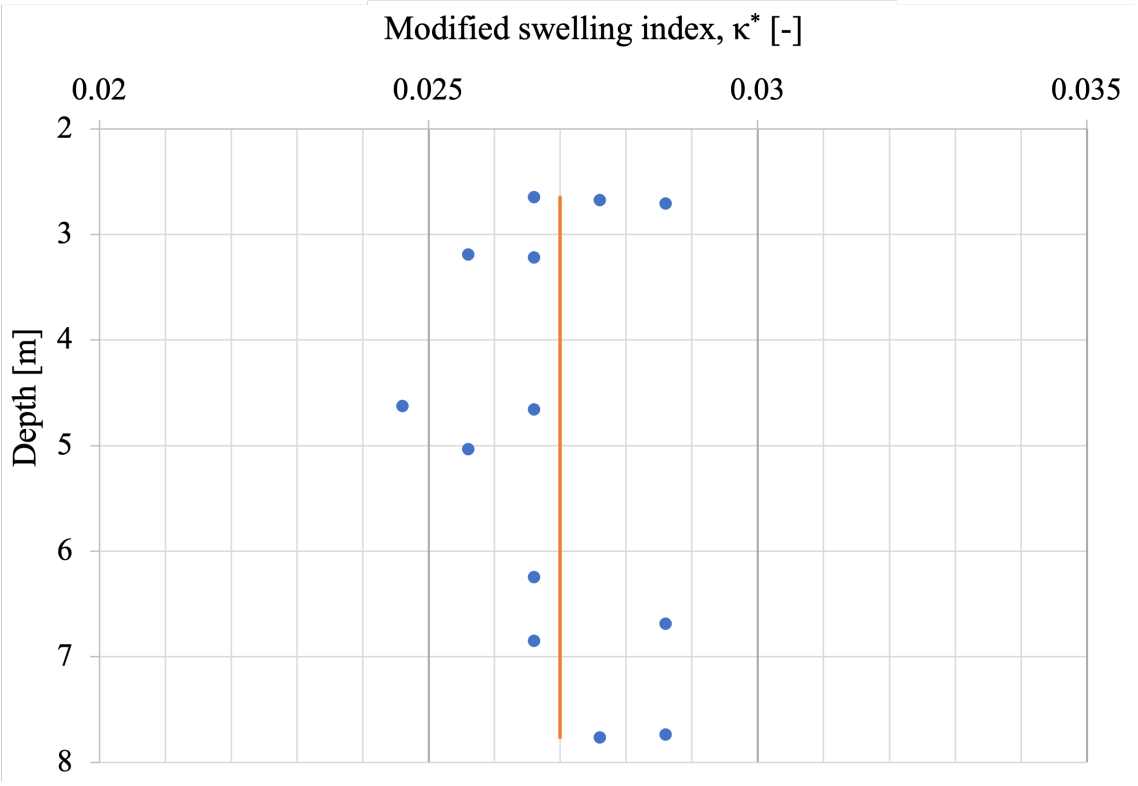

Figure A.4: κ^* of samples with good to fair quality.

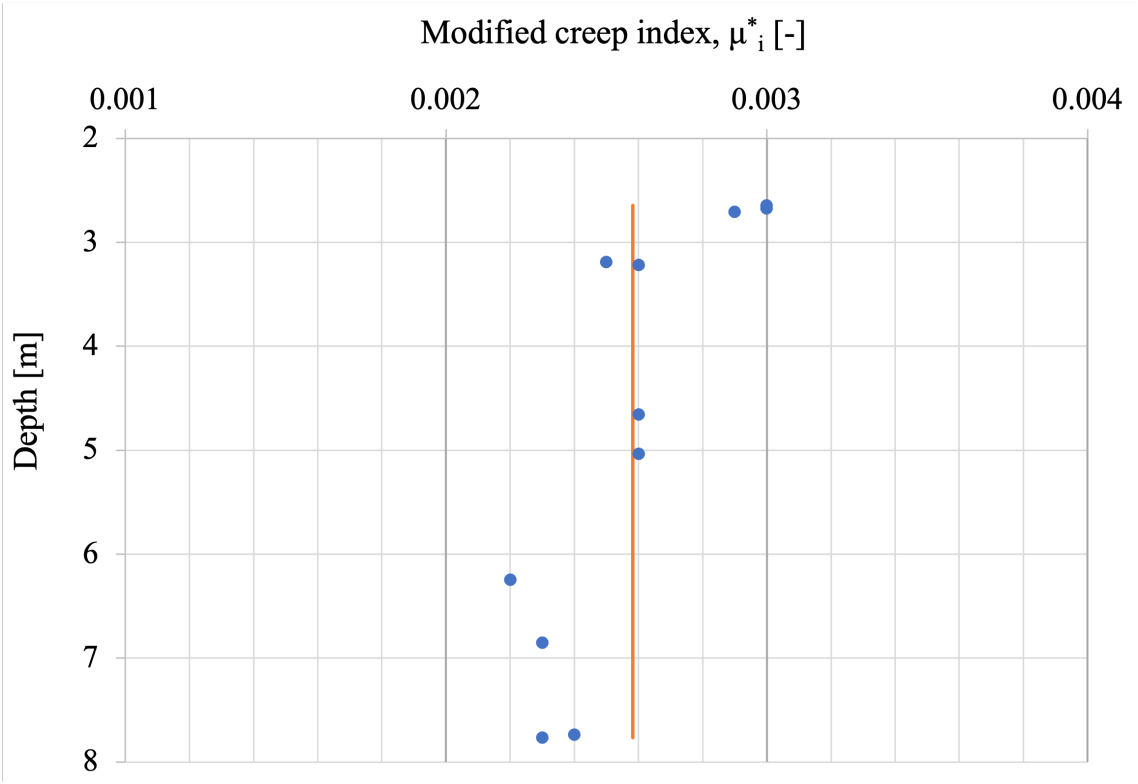

Figure A.5: μ_i^* of samples with good to fair quality.

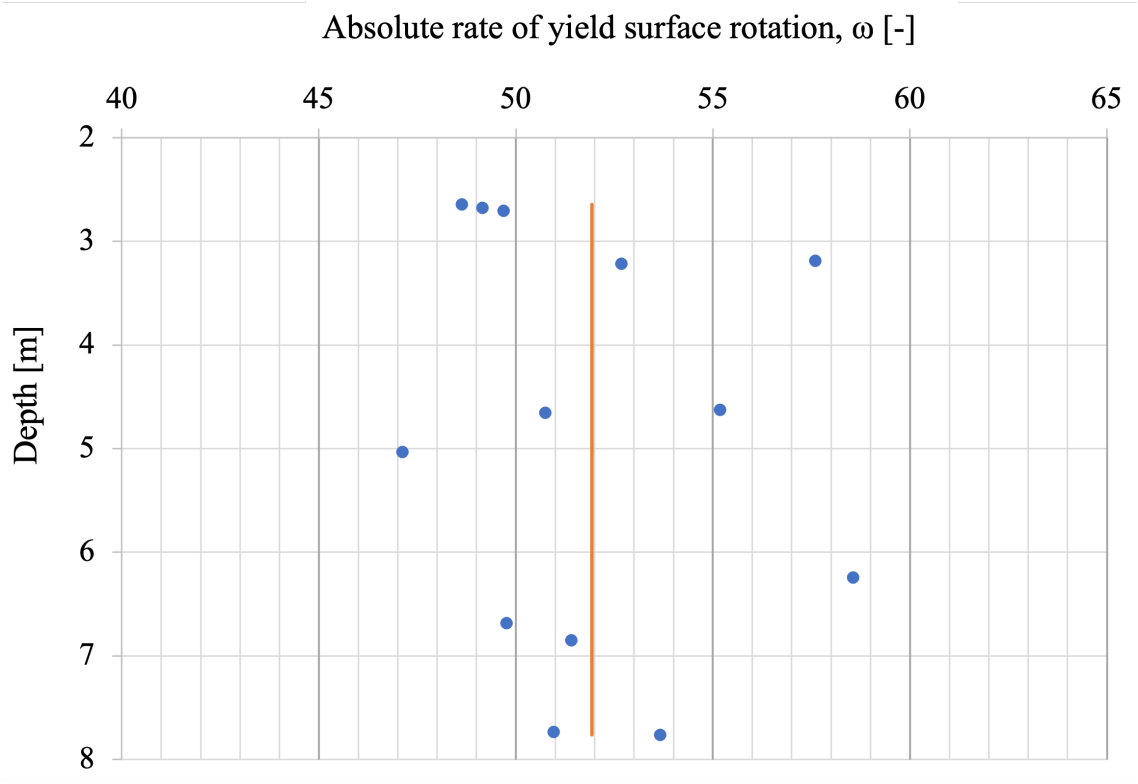

Figure A.6: ω of samples with good to fair quality.

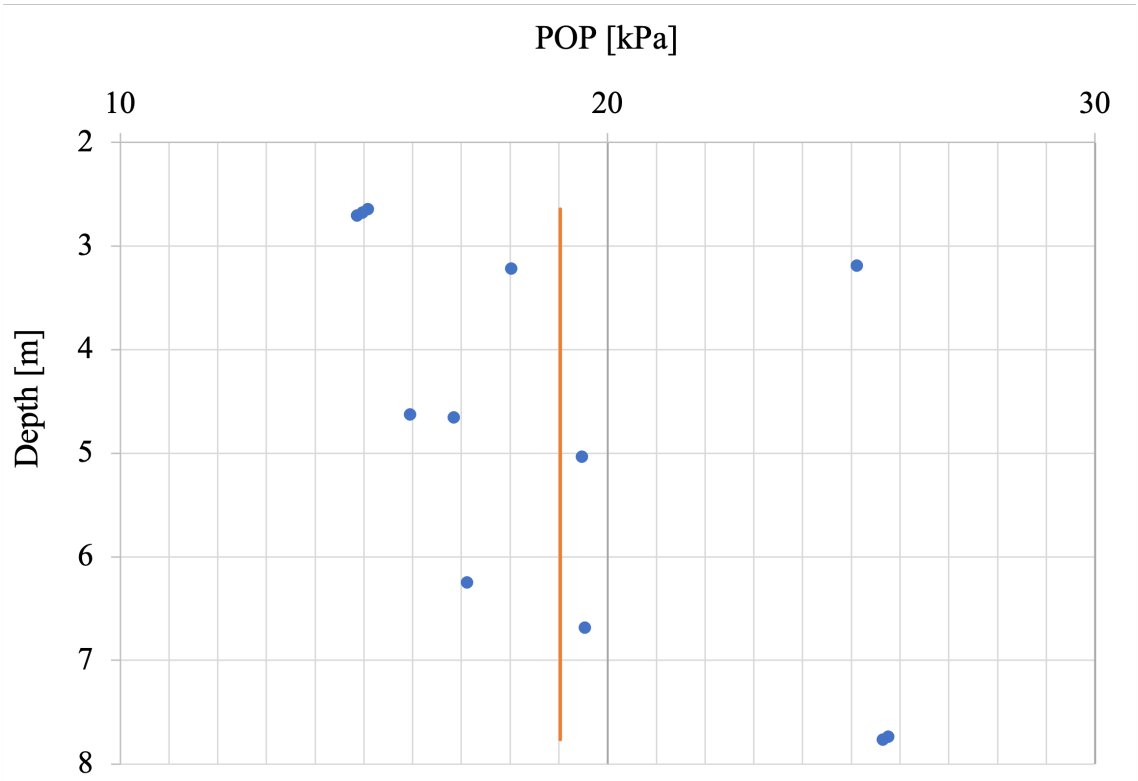

Figure A.7: POP of samples with good to fair quality.

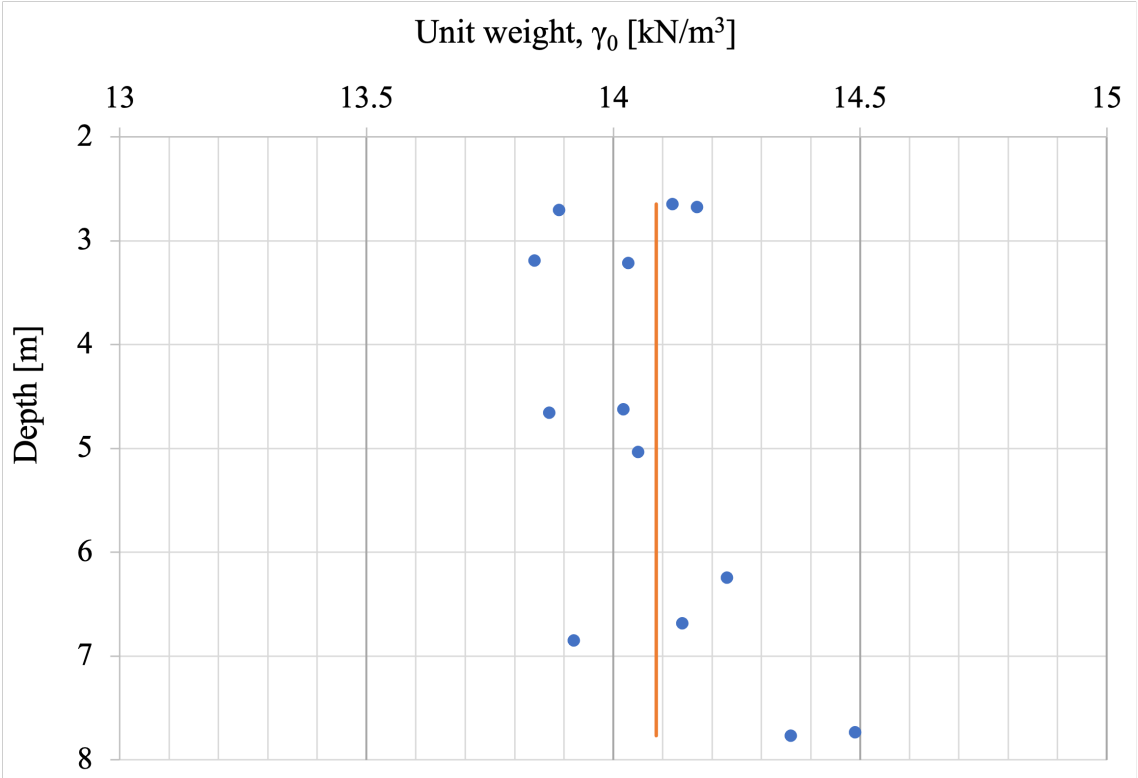

Figure A.8: Unit weight of samples with good to fair quality.

A.4 Information related to the Perniö test embankment

Table A.5: Loading steps (Lehtonen, 2011).

		Load at the end of load cycles [kPa]			
	Time of load cycles	**Container 1**	**Container 2**	**Container 3**	**Container 4**
	Start	4	4	4	4
Day 1	15:55–16:35	6.6	9.6	9.8	6.5
	16:41–17:18	11.3	14.3	14.6	11.2
	17:20–17:56	15.9	19.1	19.3	15.9
	18:13–18:49	20.7	23.8	23.9	20.6
	18:49-8:14	20.7	23.8	23.9	20.6
Day 2	8:14–8:53	24.6	29.5	29.4	24.5
	9:00–9:36	29.3	34.3	34.3	29.3
	9:39–10:14	34	39.2	39.2	34.2
	10:37–11:11	39	44.1	44.2	39.1
	11:13–11:47	43.9	49	49.1	44
	12:04–12:39	48.8	53.9	53.9	48.9
	12:41–13:15	53.7	58.8	58.8	53.8
	14:00–14:35	58.7	63.7	63.8	58.7
	14:52–15:31	63.6	68.5	68.6	63.6
	15:51–16:26	68.4	73.4	73.5	68.5
	16:46–17:27	73.3	78.3	78.4	73.4
	17:39–17:59	78.2	78.3	78.4	78.3
	18:05–18:46	83.1	83.2	83.2	83.2
	18:56–19:19	85.3	85.2	85.1	85.3
	19:26–19:34	85.3	87.3	87.1	85.3
Failure	21:28	85.3	87.3	87.1	85.3

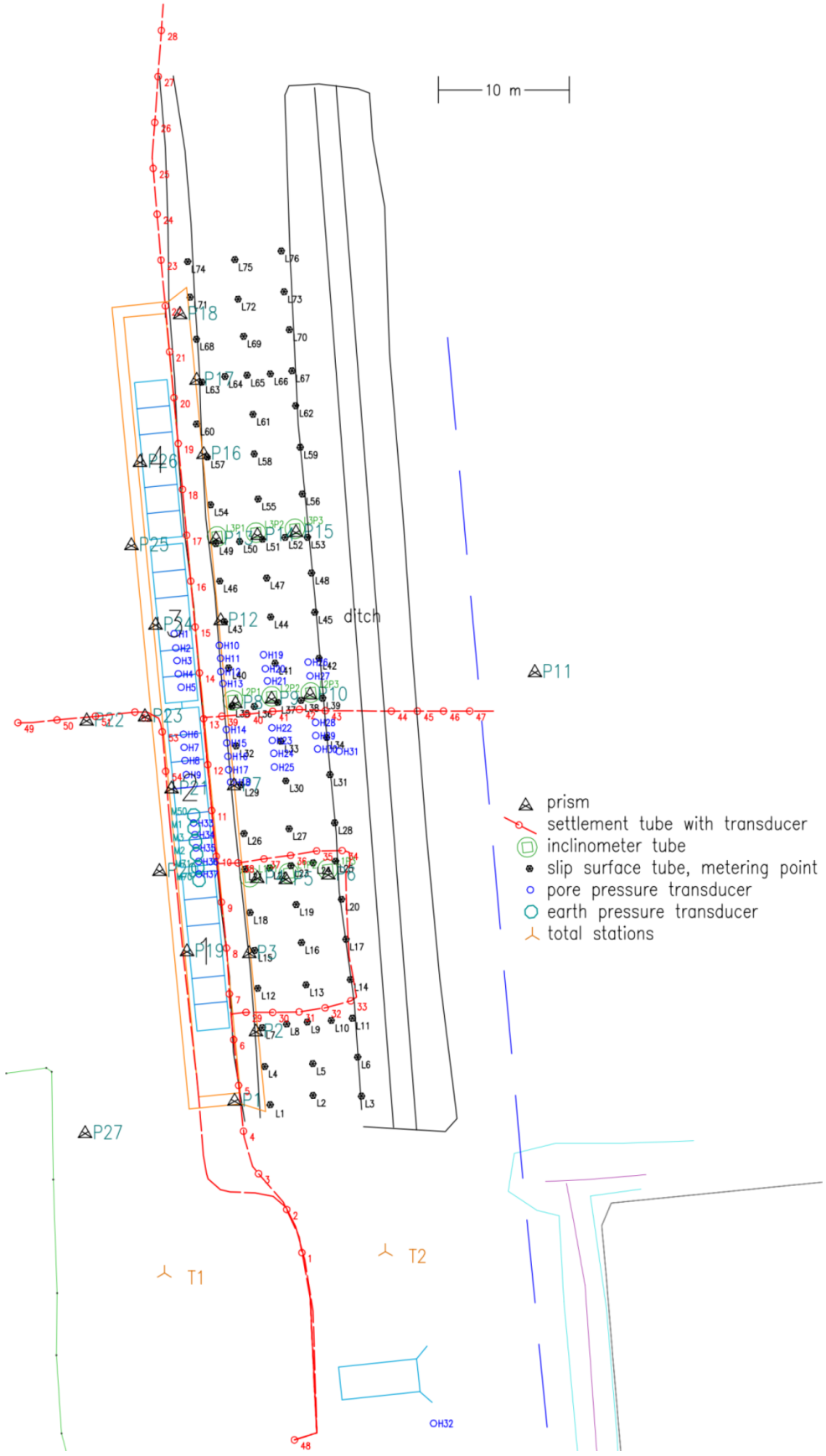

Figure A.9: Location of test instruments (Lehtonen, 2011).

A.5 Geometry of all phases

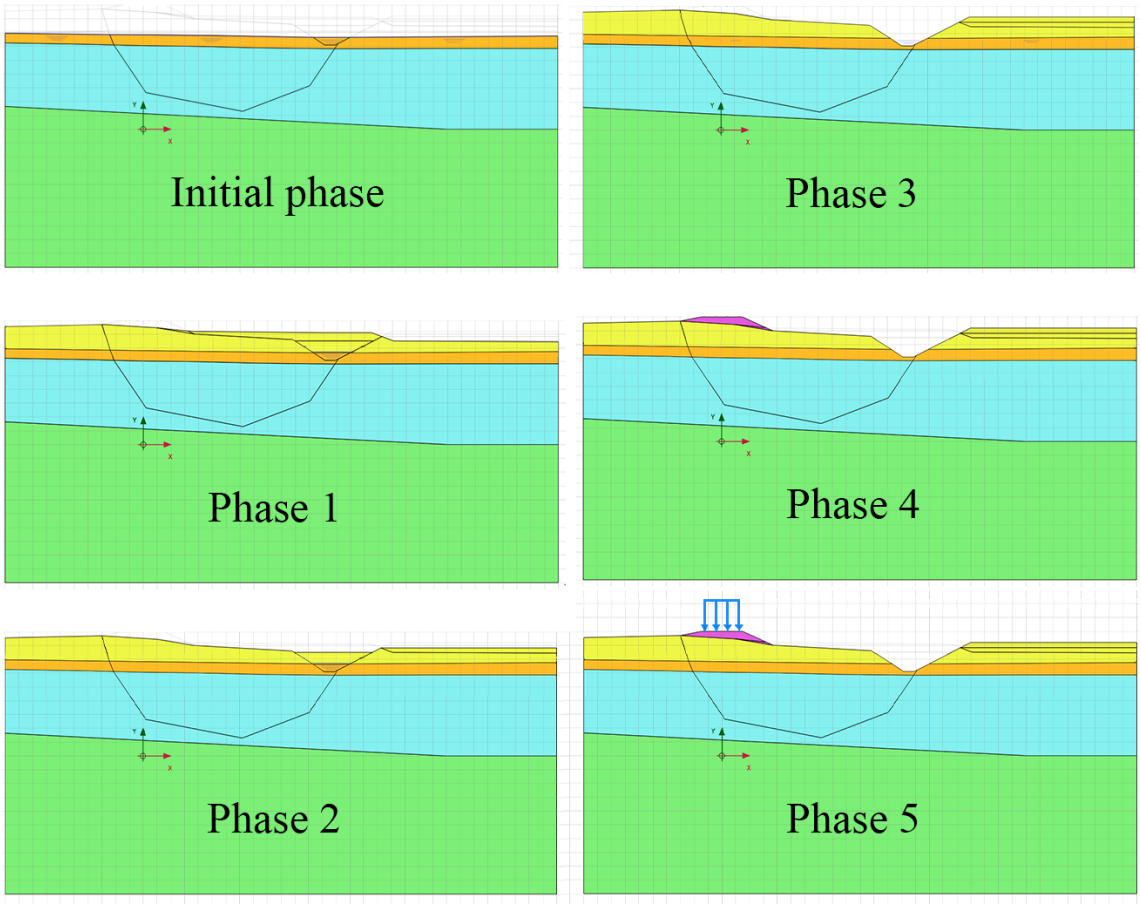

Figure A.10: Change in geometry from the initial phase to loading of the embankment.

DEPARTMENT OF ARCHITECTURE AND CIVIL ENGINEERING
CHALMERS UNIVERSITY OF TECHNOLOGY
Gothenburg, Sweden
www.chalmers.se

CHALMERS
UNIVERSITY OF TECHNOLOGY